Dear editors and reviewers,

We want to thank the reviewer for a careful and thorough reading of this manuscript and for the thoughtful comments and constructive suggestions, which help to improve the quality of this manuscript.

Minor revisions based on the reviewers' comments in the first version, as well as corrections of typos, are made this time.

Regards,

Shaoning Lv, Bernd Schalge, Pablo Saavedra Garfias, and Clemens Simmer

Required sampling-density of ground-based soil moisture and brightness temperature observations for calibration/validation of L-band satellite observations based on a virtual reality

Shaoning Lv[1*], Bernd Schalge[1], Pablo Saavedra Garfias[2], Clemens Simmer[1]

1. Institute for Geosciences ~~and-~~ Section Meteorology at the University of Bonn, Auf dem Huegel 20, 53121 Bonn, Germany; 2. Geophysical Institute at the University of Bergen, Allégaten 70, 5020 Bergen, Norway.

Abstract: Microwave remote sensing is the most promising tool for monitoring ~~global-scale~~ near-surface soil moisture distributions globally. With the Soil Moisture and Ocean Salinity (SMOS) and Soil Moisture Active Passive (SMAP) missions in orbit, considerable efforts are made to evaluate ~~their~~derived soil moisture products via ground observations, ~~forward~~ microwave transfer simulation, and independent remote sensing retrievals. Due to the large footprint of the satellite radiometers of about 40 km in diameter and the spatial heterogeneity of soil moisture, minimum sampling densities for soil moisture are required to challenge the targeted precision. Here we use 400 m resolution simulations with the regional ~~terrestrial system model~~ Terrestrial System Modeling Platform (TerrSysMP) and its coupling with the Community Microwave Emission Modelling platform (CMEM) to quantify the maximum sampling distance ~~required~~allowed for soil moisture and brightness temperature validation. ~~-~~Our analysis suggests that an overall sampling ~~resolution~~distance of ~~better~~finer than 6 km is required to validate the targeted accuracy of 0.04 cm^3/cm^3 ~~(~~with a 70% confidence level~~)~~ in SMOS and SMAP estimates over typical ~~midlatitude~~mid-latitude European regions. The ~~minimum~~maximum allowed sampling ~~resolution~~distance depends on the land-surface ~~inhomogeneity~~heterogeneity and the meteorological situation, which ~~influence~~influences the soil moisture patterns, and ranges from about ~~7~~6 km to 17 km for a 70% confidence level for a typical year. At the ~~minimum~~maximum allowed sampling ~~resolution for~~distance on a 70% confidence level ~~also~~, the accuracy of footprint-averaged soil moisture is equal or better than brightness temperature estimates ~~is equal or better than 15 K/10 K for H/V polarization.~~over the same area. Estimates strongly deteriorate with ~~sparser~~larger sampling ~~densities, e.g., at 3/9 km with 3/5 sampling sites the confidence level~~distances. For the evaluation of ~~derived footprint estimates can reach about 0.5-0.6 for soil moisture which is much less than the standard 0.7 requirements for ground measurements. The representativeness~~the smaller footprints of ~~ground-based soil moisture~~ the active and ~~brightness temperature observations – and thus their~~active/passive products od SMAP the required sampling densities increase; e.g., when a grid resolution of 3 km diameter is sampled by 3 sites of footprints of 9 km sampled by 5 sites required already only 50%-60% of the pixels have a sampling error below the nominal values. The required minimum

Style Definition: Comment Text

sampling densities ~~-~~for ground-based radiometer networks to estimate footprint averaged brightness temperature are higher than for soil moisture due to the non-linearities of radiative transfer, and only weakly correlated in space and time. This study provides a basis for a better understanding of the sometimes strong mismatches between derived satellite soil moisture products and ground-based measurements.

Key words: passive microwaves, soil moisture, brightness temperature, sampling density

1. Introduction

Information on the global soil moisture distribution is required, e.g., for weather forecasting, climate research, and ~~agriculture~~agricultural applications. Due to the high spatial variability of soil moisture, its in-situ observation is practically impossible on continental scales. Passive microwave satellite remote sensing at L-band frequencies may achieve this goal because of the strong dependency of the soil dielectric constant on soil moisture, the - compared to higher frequencies - reduced sensitivity of the brightness temperatures to surface roughness and vegetation (Njoku and Kong, 1977;Ulaby et al., 1986), and the high transparency of the atmosphere at these wavelengths ~~(Njoku and Kong, 1977;Ulaby et al., 1986).~~. The first operational L-band soil moisture detection satellite, SMOS (Soil Moisture and Ocean Salinity) was launched in 2008 (Kerr et al., 2010) and was followed in 2015 by SMAP (Soil Moisture Active Passive), which ~~additionally carries~~initially were performing with an active instrument to achieve higher spatial resolution (Entekhabi et al., 2010); the active component did fail, however, shortly after the full operation of the satellite. Both satellites are currently continuously and globally observing passive microwave brightness temperatures, from which soil moisture products are derived at ~~tens of kilometers~~a spatial resolution of 36 km and 9 km.

Before and after the launch of SMOS and SMAP several soil moisture monitoring networks for evaluation and retrieval algorithm development were ~~set up~~established, such as ESA's ~~validation~~ efforts at the Valencia Anchor Station (VAS) in eastern Spain ~~and~~, SMOSREX (Surface Monitoring Of Soil Reservoir Experiment) in France, the upper Danube watershed located in southern Germany (Delwart et al., 2008;de Rosnay et al., 2006;~~Lemaitre~~dall'Amico et al., ~~2004~~2012;Kerr et al., 2016), and the SMAP Cal/Val project (~~Brown et al., 2008;Delwart et al., 2008;~~Colliander et al., 2017a;Burgin et al., 2017;Chen et al., 2017;Chen et al., 2018)~~.~~. All those networks have been established since ground truth should be the only standard to evaluate these products. According to the Level 1 baseline and the minimum SMAP science requirements (SMAP Science Data Cal/Val Plan, (O'Neill et al., 2015)~~)~~ the spatial resolution of Level 2 (Passive Soil Moisture Product L2_SM_P) and Level 3 (daily composite L3_SM_P) soil moisture products is 36 km ~~with~~, which have to reach an accuracy for soil moisture of 0.04 cm^3/cm^3~~.~~ with a probability of 70%. A wide range of measurement techniques and protocols exist for setting up and performing ground-based observations for ~~evaluation.~~such evaluations. SMAP Cal/Val suggests, that volumetric soil moisture should be observed in-situ at 5 cm and 100 cm depth ~~while~~; optimal sensing/mounting depths are, however, still debated (Lv et al., 2016a;Lv et al., 2018;Lv et al., 2019). For core validation sites~~,~~ a minimum of six ~~- better 15 observations - over~~stations should cover one SMAP grid cell or footprint ~~is suggested~~ (O'Neill et al., 2015;Famiglietti et al., 2008)~~,~~; but this value has not ~~substantiated~~ yet been shown to guarantee the nominal accuracy by a thorough analysis (Jackson et al., 2012;Crow et al., 2012)~~.~~. More recent results show that the spatial representativeness of the soil moisture tends to increase with the timescale of data series, but so does their spread (Molero et al., 2018). For Cal/Val, it is required to have instantaneous soil moisture values rather than averages in different timescales. Relevant studies typically use ground-based soil moisture networks with fixed ~~resolutions~~average sampling distance over rather homogeneous land surfaces, which are, however, not necessarily representative for all land surface types. For SMAP core calibration/validation sites ~~a 36-km footprint~~, the data product grid-cell should be sampled with at least ~~be sampled with~~ eight stations ~~leading~~ to ~~a~~reach with 70% confidence ~~for~~ an estimated ~~mean~~ soil moisture uncertainty of 0.03 m^3/m^3 given a spatial ~~variability~~soil moisture standard deviation of 0.07m^3/m^3~~. A 9-km footprint should at least~~ as assessed from field measurements (Colliander et al., 2017b). According to the same source, grid-cells with a dimension of 9 km (as for downscaled SMAP products) should be sampled with at least five stations ~~leading to a 70% confidence for an estimated mean soil moisture uncertainty of 0.03 m³/m³, while a 3-km footprint should~~ and pixels with 3 km diameter with at least ~~be sampled with~~ three stations ~~leading~~ to ~~a~~reach with 70 % confidence ~~for~~ an ~~estimated~~accuracy of 0.03 and 0.05 m^3/m^3 ~~mean soil moisture uncertainty in both cases.~~, respectively, while assuming a spatial soil moisture ~~uncertainty~~standard deviation of 0.05 m^3/m^3 within the ~~respective footprints~~grid-cell.

(Ochsner et al., 2013)) point out that too few resources are currently devoted to in-situ soil moisture monitoring networks, and that despite their increasing number, a standard for network density and sampling procedures ~~is~~are missing. ~~Coopersmith et al., 2016 suggest~~The International Soil Moisture Network (ISMN, https://ismn.geo.tuwien.ac.at/en/) is an effort for unifying global soil moisture observation networks (Dorigo et al., 2011). (Coopersmith et al., 2016)) suggested temporary network extensions around permanent installations to quantify the representativeness of the latter. ~~-~~(Qin et al., 2013)~~) suggest~~) suggested the use of MODIS-derived apparent thermal inertia to interpolate between in-situ soil moisture measurements. So far, the required sampling density is discussed only concerning in-situ measurements, which heavily depend on sensor quality and network location (Vereecken et al., 2008;Brocca et al., 2010;Bhuiyan et al., 2018)~~. No study is known to us, which investigates systematically the station density required for the evaluation of derived soil moisture or brightness temperatures taking the true~~. Higher station numbers are necessary, as well as the establishment of general rules for their selection (Cosh et al., 2017). Chen et al. (2017, 2018, 2019) suggest the utilization of TC (Triple collocation), which is a statistic method to characterize systematic biases and random errors, or ETC (Extended Triple collocation) to analyze the noise component in soil moisture observations, and to use correlation to evaluate the representativeness of soil moisture networks. They also suggest that the core validation sites should allow validating the retrieved soil moisture to an accuracy of 0.04 cm^3/cm^3 with a probability of 70% in terms of unbiased RMSE because the bias itself is hard to eliminate.

Establishing ground monitoring networks for calibration/validation of soil moisture products from satellite L-band observations is challenging partly due to the different spatial scales between observations from soil moisture sensors and satellites. Moreover, from a direct comparison between satellite soil moisture products and ground-based measurements from existing soil moisture networks, it is impossible to isolate the sampling error, and only very few studies investigate systematically the station density required to allow for a given accuracy taking the land heterogeneity into account. In our study, we use a 400-m resolution virtual reality generated with a regional terrestrial modeling system coupled with an observation operator to estimate such minimum station densities ~~for the evaluation of L-band satellite observations and soil moisture retrieval products. This~~. The virtual reality contains realistic soil, land cover, and topography variability and allows us to arbitrarily vary the sampling ~~resolution at~~ density and, thus, average sampling distance in steps of 400 m~~, which is impossible in field campaigns.~~. Section 2 introduces ~~our model-based~~ the virtual reality, and the observation operator used to transfer the terrestrial system states into virtual observations. In Section 3, we ~~analyze~~derive the error growth with increasing average sampling ~~distances in time~~distance for soil moisture and ~~space~~brightness temperatures. Conclusions and discussion are provided in Section 4.

2. Methodology and data

2.1 Virtual reality

The modeling system used to create the virtual reality from which we draw the virtual soil moisture observations and compute brightness temperatures is the Terrestrial Systems Modeling Platform (TerrSysMP, (Shrestha et al., 2014;Gasper et al., 2014;Sulis et al., 2015) developed within the framework of the Transregional Collaborative Research Center 32 (TR32, Simmer~~,~~ et al~~.~~., 2015). TerrSysMP consists of the atmospheric model COSMO (Consortium For Small Scale Modelling, (Baldauf et al., 2011), the land surface model CLM (Community Land Model Version 3.5, (Oleson et al., 2008)~~),~~, and the distributed hydrological model ParFlow v693 (Ashby and Falgout, 1996;Kollet et al., 2010). The platform ~~has especially been~~, specially designed for high-performance computing environments (Gasper et al~~.~~., 2014~~) and~~), has been extensively evaluated against observations (Sulis et al~~.~~., 2015, 2018; Shrestha et al~~.~~., 2018b) ~~and~~as well as similar regional terrestrial system models (Sulis et al~~.~~., 2017). The effect of spatial resolution on simulated soil moisture and the resulting exchange fluxes between land and atmosphere has been studied with TerrSysMP by Shrestha et al. (2015, 2018a).

~~The simulated domain in this study is centered on the Neckar catchment in southwestern Germany (Figure 1). Notable features include the upper Rhine valley in the west, the Black Forest mountains in the southwest, and the foothills of the Alps in the southeast. The landscape has height variations of about 1100 m with lowest elevations found in the Rhine valley and highest in the Black Forest. The topographic data are~~We use for this study available simulation results generated by the research unit FOR2131 (Schalge et al., 2019;Schalge et al., 2016) over an area containing the Neckar catchment in southwestern Germany in its center (Figure 1). CLM and ParFlow were run at the horizontal computational grid with 400 m resolution. ParFlow has 50 vertical soil layers in which the upper 10 coincide with the ten soil layers of CLM. The vertical resolution is variable with smaller steps near the land surface. The atmospheric model COSMO runs at a 1.1 km horizontal resolution, and COSMO is forced at the lateral boundaries with a COSMO-DE analysis from the operational weather forecast run by the German national weather service (Deutscher Wetterdienst, DWD) available at hourly time steps. The main topographic features of the modeling area are the upper Rhine valley in the west, the Black Forest in the southwest, and the foothills of the Alps in the south. The heights range from 80 m to 1900 m. The area was selected by the research unit because of its heterogeneity in topography and land-use typical for midlatitude European river catchments; thus, it is also well suited for our study. The objective of the research unit is the setup and test of a strongly coupled data assimilation system with a fully-coupled regional terrestrial model. Their virtual reality run (VR01), the results of which we are exploiting in this study, is the so-called nature run from which the research unit draws the virtual observations to be assimilated in a lower-resolved model version using ensemble methods. The model area can be covered by about 15 x 20 SMOS pixels, which suffices for the statistical analyses performed to determine required sampling densities. There exist two soil moisture monitoring networks close to the domain, which are used for soil moisture validation studies with satellite-based L-band observations (Montzka et al., 2013).

The topographic data for VR01 is obtained from the European Environment Agency EEA (http://www.eea.europa.eu/data-and-maps/data/eu-dem), which is also the source for the CORINE land use data ~~(http://www.eea.europa.eu/data-and-maps/data/corine-land-cover-2006-raster-3)~~(http://www.eea.europa.eu/data-and-maps/data/corine-land-cover-2006-raster-3) used to characterize vegetation in the model domain. Since CORINE uses many more land~~-~~-use classes than CLM, the CORINE classes are aggregated to the five classes discriminated in the CLM in the modeling area: broadleaf forests which can be found mostly in hilly areas throughout the domain in smaller patches, needle leaf forests which dominate at higher elevation such as the Black Forest, grassland which is relatively rare and only appears in small patches, and crops which is the most dominant land use type throughout the domain and appears almost anywhere. All other classes, such as urban areas, are treated as bare soil in ~~our study~~VR01.

The Leaf Area Index (LAI) for the specific plant classes is taken from MODIS estimates corrected for known biases (Tian et al., 2004). ~~We have not used the tiling approach in CLM; instead, we used the most dominant land use type for each grid-cell because the resolution is high enough to warrant this approach. The SAI is estimated from the LAI by a slightly modified formulation (no dead leaf for crops, constant base SAI of 10 % of maximum LAI) by~~Instead of the tiling approach implemented in CLM, the dominant land use type for each grid-cell is used, because the resolution of 400 m is high enough to warrant this approach. The SAI (Stem Area Index) is estimated from the LAI by formulations slightly modified from those implemented in the CLM. For crops, SAI is just 10% of the LAI; thus SAI is larger in summer than in winter. For all other types, SAI is 10% of LAI plus a "dead leaf" component. The “dead leaf" component is estimated empirically from the change of the LAI from the previous and current month. The “dead leaf" component is only a major contributor during fall, but even there the needle leaf trees, for instance, show only a small increase of SAI. The VR01 region is mostly covered by deciduous trees that have 1-2 months of high SAI because the dead-leaf component decays rather quickly. Details about SAI calculation in VR01 are described in (Schalge et al., 2016)), (Lawrence and Chase, 2007)), and (Zeng et al., 2002)~~.~~).

Formatted: English (United Kingdom)

The soil map (Figure 1, upper row) is derived from a product of the German Federal Institute for Geosciences and Natural Resources BGR (http://www.bgr.bund.de/DE/Themen/Boden/Informationsgrundlagen/Bodenkundliche_Karten_Datenbanken/BUEK1000/buek1000_node.html). Soil values for regions near the edge of ~~our domain in France and Switzerland were extrapolated. Variability~~

~~was added to the relatively large polygons of constant soil parameters following Baroni et al. (2017) to represent better what would be found in reality at higher resolutions. The soil color was~~the modeling domain in France and Switzerland are extrapolated. Variability was added to the relatively large polygons of constant soil parameters to represent better what would be found in reality at higher resolutions following (Baroni et al., 2017). The soil color is derived from the carbon content of the soil with carbon-rich soils being darker, except for the bare soil areas~~,~~ which all use the same relatively light color class. There is deep soil geology included in ParFlow as well as alluvial channels below rivers to account for deeper subsurface flow~~,~~; but these features will not directly impact the results shown here as they only appear below the soil layers.

~~CLM and ParFlow use the same horizontal computational grid with 400 m resolution. ParFlow has 50 vertical soil layers, the upper 10 of which coincide with the ten soil layers of CLM.~~

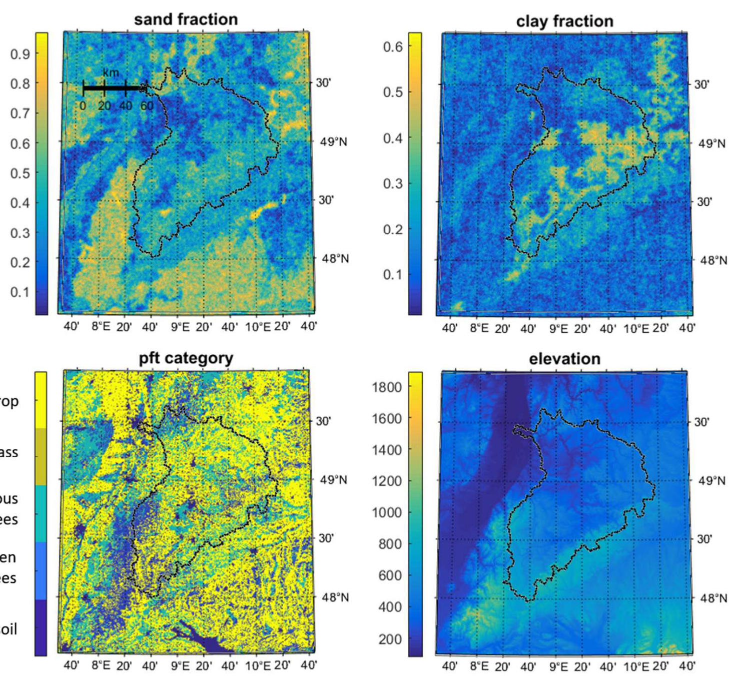

Figure 1: TerrSysMP simulation area at 400 m resolution with the Neckar catchment roughly in the center indicated by the black line. Soil sand (left) and clay fractions (right) are displayed in the upper row sub-figures, while the Plant Functional Types (PTFs) used by CLM are shown in the lower left sub-figure, and topography (in m) in the lower right sub-figure.

~~The vertical resolution is variable with smaller steps near the land surface. The atmospheric model COSMO runs at a 1.1 km horizontal resolution which allows for convection permitting simulations. COSMO is forced at the lateral boundaries with a COSMO-DE analysis from the operational weather forecast runs from the German national weather service (Deutscher Wetterdienst, DWD) available at hourly time steps.~~

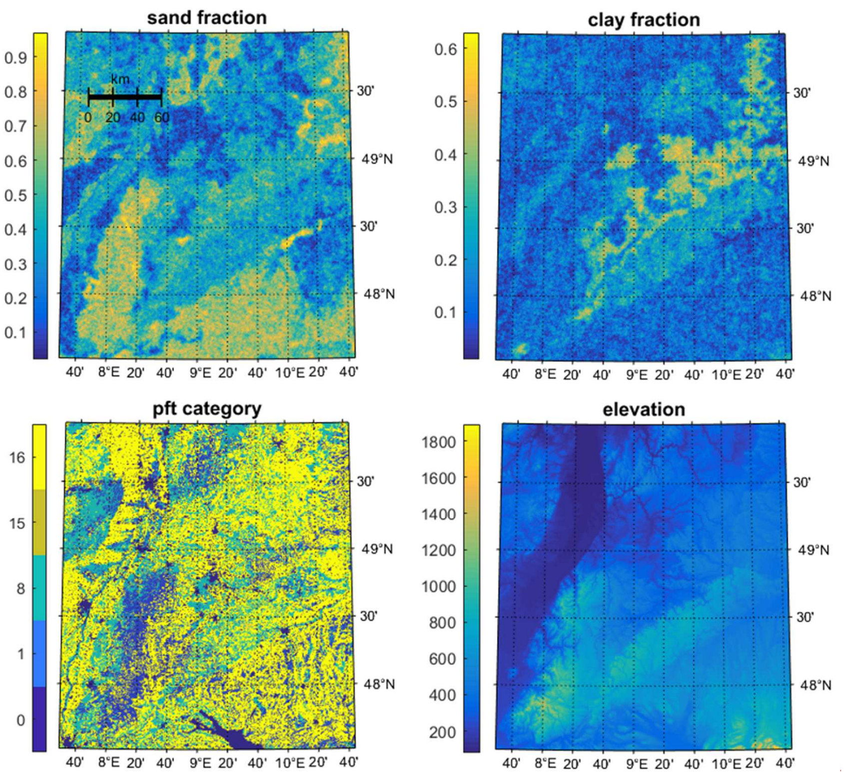

~~Figure 1: TerrSysMP simulation area at 400 m resolution with the Neckar catchment roughly in the center. Soil sand (left) and clay fractions (right) are displayed in the upper row sub-figures, while the Plant Functional Types (PTFs) used by CLM are shown in the lower left sub figure (here we use a discrete scale representing the five classes including: 0 bare soil; 1 needle leaf evergreen temperate trees; 8 broadleaf deciduous temperate trees; 15 warm c4 grass; 16 crop) and topography (in m) in the lower right sub-figure.~~

2.2 Generation of L-Band passive microwave observations

The radiative transfer model CMEM (Rosnay et al., 2009) computes the land emissivity based on a dielectric mixture model for soil moisture, soil sand and clay ~~soil~~ fractions, soil surface roughness, vegetation optical thickness, single scattering albedo, and land surface orientation relative to the satellite viewing perspective. Depending on the sand and clay fractions, brightness temperatures may vary by tens of Kelvins given the same near-surface soil moisture. Vegetation optical thickness depends on LAI, which varies in ~~our virtual reality with time depending on PFT type. Also, soil temperature and snow depth (not shown) impact the simulated brightness temperatures. More details can be found, e.g.,~~the VR01 with time depending on PFT type. Depending on the particular Plant Functional Type (PFT) CMEM uses different parameters to calculate the vegetation optical thickness from the respective LAI. Soil effective temperature is computed with a new scheme introduced by (Lv et al., 2014). The new scheme is a discretization of the integral formulation and takes advantage of multi-layer soil temperature/moisture profile information with a wider range of soil properties. This allows to better adapt CMEM to the available land surface model data. Also, soil temperature and snow depth impact the simulated brightness temperatures. More details can be found in the SMOS global surface emission model handbook (Rosnay et al., 2009).

From the 400 m resolution brightness temperatures, virtual satellite observations are generated with CMEM taking the satellite antenna function into account. Figure 2 shows the centers of the about 320 footprints ~~covering~~corresponding to the ~~model area~~SMOS L1 TB data product at 41° incidence angle for ~~one~~a potential satellite overpass and - on the same scale - the satellite antenna function for one footprint, which ~~will change somewhat in~~changes shape ~~with~~depending on the elevation of the individual 400 m model grid areas, orbit altitude and declination, and satellite ~~viewing~~scanning and incidence angle.

Not each SMOS overflight will cover the whole area in reality. But in our study, we assume for simplicity, that all footprints indicated in Figure 2 are observed once a day at 6 a.m~~.,~~. local time, which corresponds to the approximate ascending and descending~~ or ascending~~ overpass time of SMOS and SMAP, respectively. The satellite footprint is much larger than the nominal satellite spatial resolution of 40 km that is defined by 3 dB contour of the main lobe; thus areas much larger in diameter contribute to one satellite-observed brightness temperature (i.e., 50% of one satellite-observed brightness temperature originates from an area roughly ten times larger than the nominal satellite footprint).

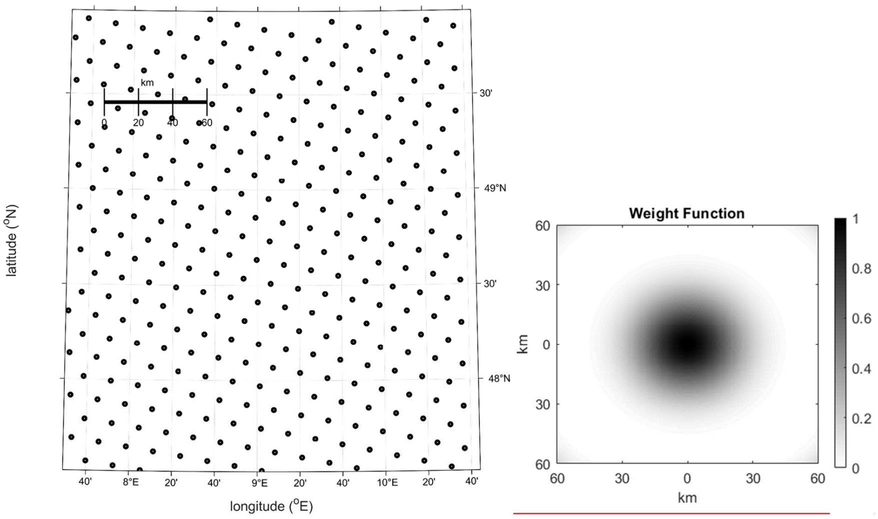

~~Figure 2: Dots in the left sub figure indicate the centers of SMOS footprints for one hypothetical satellite overpass. The right sub-figure shows the antenna pattern in dB of one satellite footprint on the same scale as the map on the left.~~

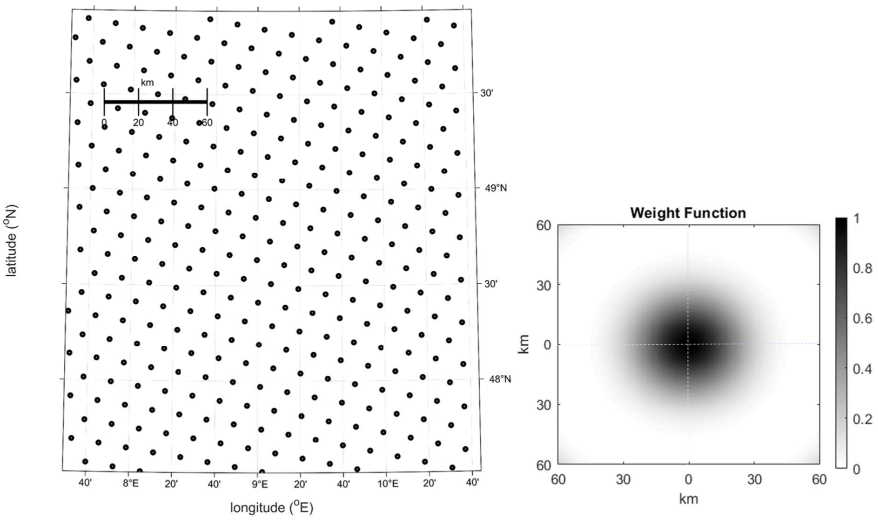

Figure 2: Dots in the left sub-figure indicate the centers of SMOS footprints for one hypothetical satellite overpass. The right sub-figure shows the antenna pattern of one satellite footprint at nadir on the same scale as the map on the left sub-figure.

The virtual reality employed in this study is a physically consistent state of the terrestrial system in space and time because it has been produced by a numerical model based on the conservations equations for mass, energy, and momentum. When applying the satellite observation operator ~~CMEM~~ to this model state, we assume that the model state is correct~~ and~~, as well as the simulated ~~microwave transfer is error-free.~~brightness temperature. Thus, our ~~sampling~~ study only quantifies the impact of the sampling density ~~but does not include~~of a surface network on the comparison between area-averaged values and their estimates from the surface network, i.e., we ignore errors of the dynamic model (TerrSysMP) and~~/or~~ of the forward operator (CMEM). Based on the modeling results, we analyze a range of ground-based network configurations with sampling points at least 400 m apart, and we assume that all quantities (state of the terrestrial system and brightness temperature) do not vary within 400 m. While this is an approximation, we believe that our results and their outcome can be generalized~~, except that their outcome might be too optimistic.~~. We will come back to this point in the discussion section.

~~With the model area covering~~Since one SMOS/SMAP footprint ~~containing~~covers approximately 106x106 model grid columns~~, that~~ in the VR01, the respective area ~~could~~can be sampled by one up to a maximum of 106x106 (virtual) sites. If the ~~foot-print~~footprint area is sampled with n sites, there are $\cancel{C^{n}_{106x106}}$ $C^{n}_{106x106}$ sampling combinations (SC, hereafter) possible, with

Field Code Changed

~~$$SC = C^{n}_{106x106} = \frac{106!}{n!\times(106-n)!}$$~~

$$SC = C^{n}_{106x106} = \frac{106^2!}{n!(106^2-n)!} \tag{1}$$

which is an unordered, non-overlapping collection of distinct elements of a prescribed size taken from a given set. For example, with ~~an average~~a 10 km distance between sampling sites~~ of 10 km~~, about 6x6 sampling sites are possible within one footprint, which can be spatially distributed in ~~$C^{6x6}_{106x106} \approx 1.69\times10^{104}$~~ $C^{6x6}_{106x106} \approx 1.69\times10^{104}$ ways. It is computationally not feasible to consider all those combinations. When~~ we divide~~, however, we first divide each footprint into equally-sized sub-areas~~,~~ each containing exactly one sampling site (this assumes a certain degree of homogeneity within the network (which would in reality also be strived for), the number of potential sampling networks is drastically reduced. If we set~~, e.g.,~~ the ~~average~~ sampling distance ~~of~~within a 43~~-km wide footprint~~ x 43 km^2 area to i km, we divide the footprint into ~~$\left(\frac{43}{i}\right)^2$~~ $\left(\frac{43}{i}\right)^2$ sub-areas each containing ~~$106\times106\Big/\left(\frac{43}{i}\right)^2 \approx 6.08\times i^2$~~ $106\times106\Big/\left(\frac{43}{i}\right)^2 \approx 6.08\times i^2$ 400m-resolution model columns. When we further select within each of the equally-sized sub-~~area~~areas of a satellite footprint the same model column (i.e., the one with row number k and column number l both, e.g. starting at 1 in the upper left column of each subarea), a regular equidistant observation network within the SMOS/SMAP footprints is enforced similar to~~, e.g.,~~ the one used in the study by (Famiglietti et al., 2008). For each footprint (subscript f) at a particular time (subscript t) of a certain sampling distance (i km, subscript d), the number of network configurations SC_{ftd} ~~for soil moisture~~ is

~~$$SC_{ftd} = \left(\frac{i}{0.4}\right)^2 \approx 106\times106\Big/\left(\frac{43}{i}\right)^2$$~~

$$SC_{ftd} = 106\times106\Big/\left(\frac{43}{i}\right)^2 \approx \left(\frac{i}{0.406}\right)^2 \tag{2}$$

This results for a certain sampling distance (i km) for all 320 footprints and all 365 days of a year to a sample size of

~~$$SC_{ft} = \left[106\times106\Big/\left(\frac{43}{i}\right)^2\right]\times365\times320$$~~

$$SC_{ft} = \left[106\times106\Big/\left(\frac{43}{i}\right)^2\right]\times365\times320 \tag{3}$$

from which we will compute the PDF of the resulting sampling errors. For each day given ~~two observations~~one observation per day for all 320 footprints and summed over all sampling distances, we get samples of size

Field Code Changed

Field Code Changed

Field Code Changed

Field Code Changed

Formatted: Font: Italic

Formatted: Font: Italic

Field Code Changed

Field Code Changed

Formatted: Justified

$$\cancel{SC_{td} = \sum_{i=0.8,1.2...}^{18}\left[106\times106\Big/\left(\frac{43}{i}\right)^2\right]\times320}\; SC_{td} = \sum_{i=0.8}^{18}\left[106\times106\Big/\left(\frac{43}{i}\right)^2\right]\times320 \,, \qquad (4)$$

Field Code Changed

~~and for~~from which we will compute PDFs of the maximum allowed sampling distances. For each ~~satellite footprint~~grid-cell with ~~two observations~~one observation per day taken over one year and summed over all sampling distances, we get

$$\cancel{SC_{fd} = \sum_{i=0.8,1.2...}^{18}\left[106\times106\Big/\left(\frac{43}{i}\right)^2\right]\times365}\; SC_{fd} = \sum_{i=0.8}^{18}\left[106\times106\Big/\left(\frac{43}{i}\right)^2\right]\times365 \qquad (5)$$

Field Code Changed

samples, from which we determine the ~~one with~~ spatial distribution of the maximum allowed sampling ~~error~~distances. E.g., for 800 m sampling distance, we determine the maximum from $\cancel{\left(\frac{0.8}{0.4}\right)^2 \times 365\times 320 = 467200}$ $\left(\frac{0.8}{0.4}\right)^2 \times365\times320 = 467200$ samples, the number of which increases with the square of the sampling distance. ~~This~~

Field Code Changed

The sampling described above is applied to ~~both~~ soil moisture ~~and~~ (brightness temperature) with ~~and~~ (without) considering the satellite weighting function (Figure 2b). ~~The confidence level required by~~Since SMAP Cal/Val ~~in core sites is 70%. Thus, instead of~~requires that the ~~maximum error,~~nominal accuracy of 0.04 cm^3/cm^3 for retrievals should be met with a probability of 70%, we take the error at the ~~70~~70th percentile, if not specified otherwise. In the following, we mostly use the more intuitive sampling distance (km), but also the sampling density (sites per km^2) when we are qualifying tendencies. The relationship between the sampling distance and the sampling density is simply

$$\text{sampling density} = \frac{1}{\text{sampling distance}^2} \qquad (6)$$

Field Code Changed

E.g., the 15/5/3 sites for grid-cells with diameters of 36/9/3 km recommended by SMAP Cal/Val would be around 0.0116/0.0617/0.3333 sites per km^2 and correspond to a sampling distance of 9.295/4.025/1.732 km. We note here that the grid size of the SMAP passive soil moisture product is 36 km x 36 km per pixel, which is the ISEA-4H9 discrete global grid for SMOS (43 km x 43 km). The 43 km in all equations shall be exchanged by 36 km when computing the number of sampling networks by equations (1) to (3).

Formatted: Normal, Justified, Line spacing: Multiple 1.25 li

Formatted: English (United Kingdom)

3. Results

We first discuss in detail the results for soil moisture sampling. Then we extend the same methodology to brightness temperature and compare both results. We also evaluate the potential sampling error for "footprints" with grid sizes of 3 km and 9 km ~~satellite footprint sizes~~, because the SMAP products also include combined active-passive soil moisture retrievals at higher spatial resolutions (e.g., EASE-grid 9 km) and a product only based on the active sensor (EASE-grid 3 km). Two kinds of percentages are used in this study. One is the confidence level, which is related to the number of potential network configurations for one footprint as given by Equation (2)~~(2)~~. The other percentage is related to the PDF of the maximum allowed sampling distance with a confidence level of 70% (we also use 100% for comparison), which is based on Equation (3)~~(3)~~/(4)~~(4)~~/(5)~~(5)~~. The site numbers defined by SMAP are equivalent to the latter.

3.1 Soil moisture

We compare the true (but virtual) spatial arithmetic average of soil moisture at the SMOS/SMAP resolution with the arithmetic average of soil moisture at 0.05 m depth computed from the sampling points taken at ~~average~~ distances ranging from 400 m (i.e., each ~~TerrSysMP~~VR01 grid column, no sampling error) to 18 km (about half the radius of a SMAP or SMOS pixel. ~~By Equation (3), (4), and (5),~~First, we analyze the probability density function of the sampling error as it varies with the sampling distance, taking the SC_{ft} samples for one whole year of all footprints in the ~~terms of Probability density function (Figure~~whole model area into account (Equation (3)~~(3)~~, Figures 3 and 6~~,~~). Then we analyze the evolution over the year of the daily PDF of the maximum allowed sampling distance (for keeping the sampling error below the nominal value of 0.04 cm^3/cm^3 with 70% confidence) from SC_{td} samples (Equation (4)~~(4)~~, Figures 4 and 7). Finally, we look at the spatial variability of the maximum allowed sampling distance (for keeping the sampling error below the nominal value of 0.04 cm^3/cm^3 with 70% confidence) based on ~~SC_{ft}),along time dimension (Figure 4 and 7, based on SC_{td}) and along spatial dimension (Figure~~ all samples of one SMOS/SMAP pixel over the year SC_{fd} (Equation (5), Figures 5 and 8~~, based on SC_{fd}).~~). When we ~~later compare~~ analyze the sampling errors for brightness temperatures, we use footprint averages weighted by the antenna function; using ~~that strategy also~~the weighting function according to the dB pattern for soil moisture leads to differences below 0.01 cm^3/cm^3; thus, the averaging procedure does not impact our conclusions for soil moisture.

~~For each average sampling distance, we~~ We compute ~~for~~ the maximum sampling error for each sampling distance and each footprint ~~the maximum sampling error obtained~~ from the ~~twice~~ daily observations over one year of all network configurations. The ~~distribution~~distributions of the corresponding 320 values ~~is~~are displayed in the box-whisker plots in Figure 3 (top). Thus each value entering the distribution at a given ~~average~~ sampling distance (individual box-whisker plot in Figure 3) stems from that sampling network for one of the 320 SMOS~~/SMAP~~ footprints, which leads to the largest sampling error taking all ~~twice~~ daily observations over a year into account (Equation (3)~~(3)~~). With a sampling distance of 400m, we exactly reproduce the true (but virtual) arithmetic soil moisture average, i.e., the maximum error is zero. Maximum errors naturally increase with sampling distance, as demonstrated by the widening of the maximum error distribution. The median of the maximum sampling error increases ~~about~~almost linearly, with about 0.022 cm^3/cm^3 per kilometer increase in sampling distance. The spread of the maximum error increases from less than 0.01 cm^3/cm^3 at 0.8 km to approximately 0.4 cm^3/cm^3 at 18 km, with quite some variability between the sampling steps. To guarantee ~~an absolute~~a sampling error below 0.04 cm^3/cm^3 (the assumed accuracy of SMOS/SMAP retrievals) ~~, which~~ with 100% confidence everywhere in the region at any time of the year~~,~~ (Figure 3, top), the maximum ~~average~~ sampling distance should not exceed 2.8 km. ~~At an average sampling distance of~~ With a 4.8 km sampling distance, for 50% of the ~~SMOS/SMAP pixels sampling networks exist, which would lead to the occurrence of~~area and/or days of the year, we get sampling errors above 0.04 cm^3/cm^3 ~~at least once per year.~~. At ~~an average~~a sampling distance of 4.4 km (~~less than~~about 18 sites within a 43 km x 43 km pixel), the same would hold for ~~more than 75% of the SMOS pixels. We note here that the size of the average footprints of the SMAP passive soil moisture product is 36 km x 36 km per pixel which is somewhat less than for SMOS.~~ only 25% of the satellite pixels.

~~For SMAP CAL/VAL core validation sites the target accuracy should be reached with a confidence level of only 70%.~~ Figure 3 (bottom) displays the ~~distribution~~PDF of the ~~70~~maximum sampling error corresponding to the 70th percentile of the sampling error ~~at~~PDF computed for each satellite pixel ~~instead of the maximum error (100 percentile) shown in Figure 3 (top).~~ over the year. Thus, to guarantee ~~an~~a sampling error below 0.04 cm^3/cm^3 for all network configurations for only up to 70% of all ~~SMOS/SMAP~~ pixels and all days of the year, a minimum sampling distance of 6 km is required. At ~~an average~~a sampling distance of 12 km, already only 50% of the pixels fulfill this requirement. Overall, about one-quarter of the ~~nominal~~ stations ~~are~~required for 100% confidence is needed, when the requirement to stay within the 0.04 cm^3/cm^3 error margin is relaxed ~~from 100% confidence level~~ to 70%.

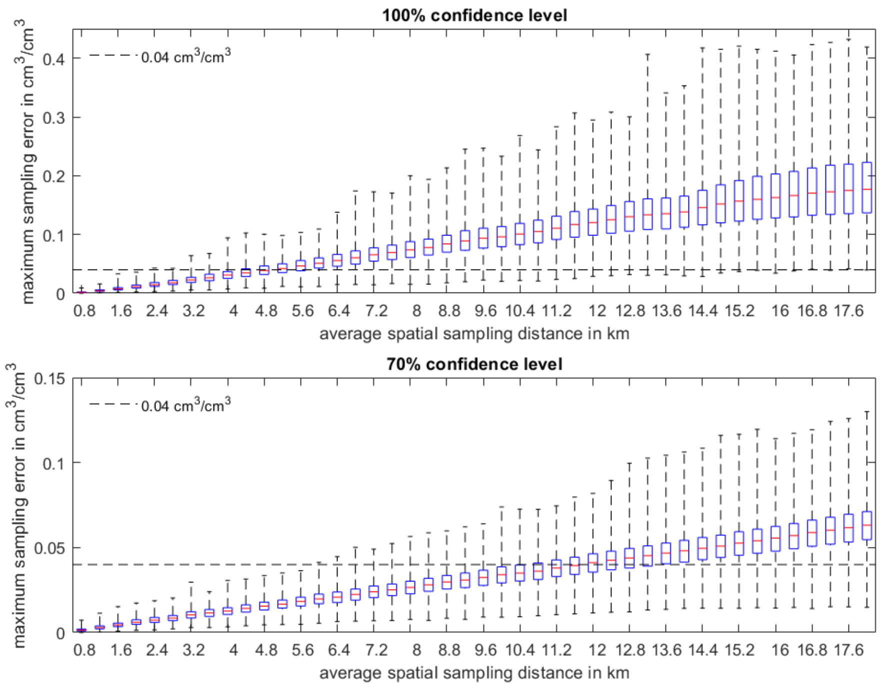

~~Figure 3: Box-whisker-plots (median in red, 25- and 75-percentiles as bounds of the box, whiskers encompass all values) of the maximum sampling errors for the 320 satellite footprints of the arithmetic mean soil moisture estimated for all network configurations observing twice a day over one year at given average sampling distances (abscissa). The top subfigure shows the absolute maximum error, while the bottom subfigure displays the results for the 70^th^ percentile of the error at each satellite footprint. The horizontal dashed line is the 0.04 cm³/cm³ retrieval error anticipated for SMOS and SMAP.~~

~~From the simulations~~

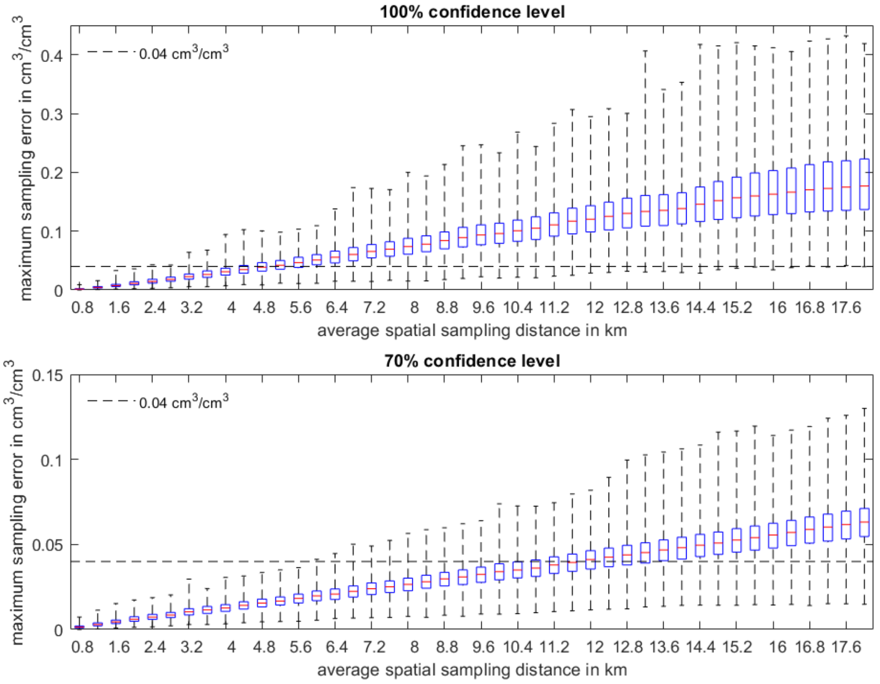

Figure 3: Box-whisker-plots (median in red, 25th- and 75th-percentiles as bounds of the box, whiskers encompass all values of the maximum sampling errors for the 320 satellite footprints of the arithmetic mean soil moisture estimated for all network configurations observing twice-a-day over one year at the given sampling distances (abscissa). The top subfigure shows the absolute maximum error, while the bottom subfigure displays the results for the 70th percentile of the sampling error distribution at each satellite footprint. The horizontal dashed line is the 0.04 cm^3/cm^3 retrieval error anticipated for SMOS and SMAP.

As outlined above, we can also quantify from the ~~required~~simulations the allowed maximum sampling distance ~~for each~~on a daily ~~observation of the whole area, and for each of~~basis from the ~~320 SMOS/SMAP footprints over time~~samples with the size given by ~~the samples defined in~~ Equation (4)~~(4)~~. According to Figure 4~~,~~ (bottom), for 80 ~~percent~~% of the SMOS/SMAP pixels, the maximum allowed sampling distance is between 8.4 km and 16 km, which is 7 - 26 stations for SMOS (43 km) and 5 - 18 stations for SMAP passive (36 km) to ~~reach the~~keep the sampling error below 0.04 cm^3/cm^3 with 70% confidence~~ level~~. A seasonal variation is not obvious, but rainfall events (Figure 4, top) affect the distributions by increasing the maximum allowed sampling distances because the surface soil moisture becomes more homogeneously distributed in space~~.~~ due to the typically quite widespread precipitation in that region. The opposite occurs during ~~drought events,~~dry periods because ~~of~~ evaporation, draining, and runoff ~~tends~~over various soil and land cover types tend to create spatially ~~inhomogeneous~~heterogeneous soil moisture distributions~~.~~, which typically reaches its maximum at intermediate soil moisture levels (Brocca et al., 2010).

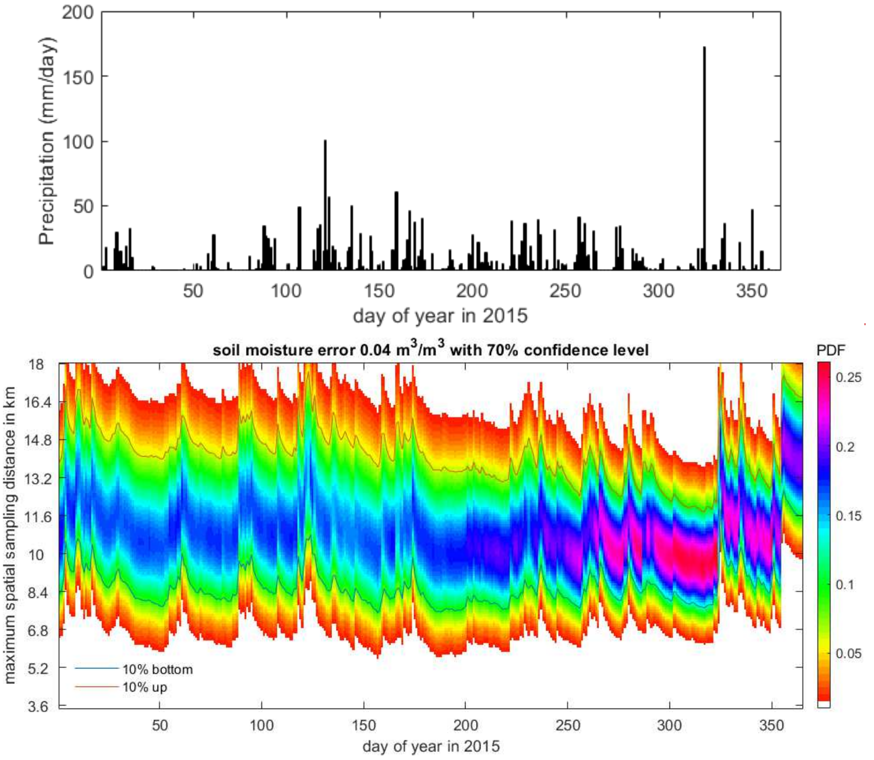

~~Figure 4: Time series of the distribution of the maximum soil moisture sampling distance for each SMOS/SMAP pixel required to assure a sampling error below 0.04 cm³/cm³ (70% confidence) for the year 2015. The grey intensity is proportional to the probability of occurrence. Also the median and the 5 and 95-percentiles are indicated as lines.~~

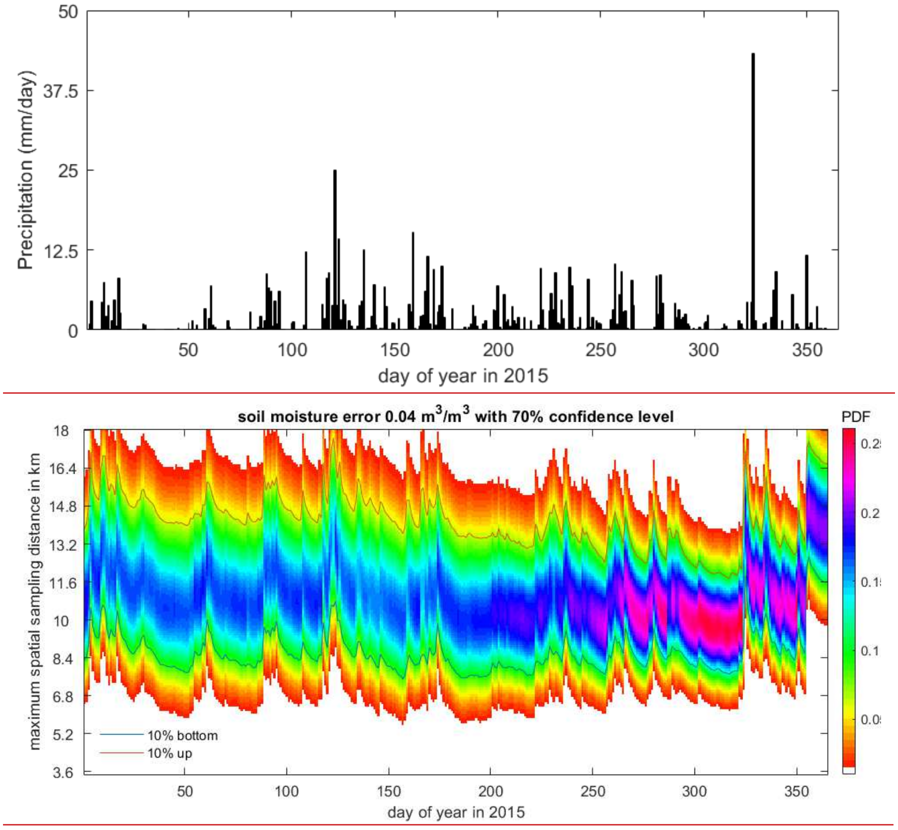

Figure 4: Precipitation in VR01 (upper panel), and time series of the distribution of the maximum allowed soil moisture sampling distance for each SMOS/SMAP pixel to assure a sampling error below 0.04 cm^3/cm^3 (70% confidence) for the year 2015 (bottom panel),. The colored intensity is proportional to the probability of occurrence. The 10th and 90th-percentiles are indicated as blue and read lines,

The spatial distribution of the annual ~~average~~ maximum sampling distance ~~required~~allowed to guarantee a sampling error below 0.04 cm^3/cm^3 ~~(~~with 70% confidence computed from the samples given by Equation (5) and its RMS for the year 2015 (Figure 5) indicates~~,~~ that the southeastern region requires ~~on average~~ sampling distances of ~~up to~~only below 16 km; thus only nine sites are required within a SMOS/SMAP pixel to estimate the footprint-averaged soil moisture with a sampling error below 0.04 cm^3/cm^3. ~~However~~Also, the annual variation is particularly small (blue). For the rest of the region, maximum allowed sampling distances range from 7 km to 10 km~~;~~ (radius); thus,~~ many~~ more than nine sites are required within one footprint. The annual variation of the maximum sampling distances for those footprints is larger than in the southeast. The mean allowed sampling distances and their day-to-day variations are only weakly correlated (correlation coefficient 0.40), but show larger-scale common patterns.

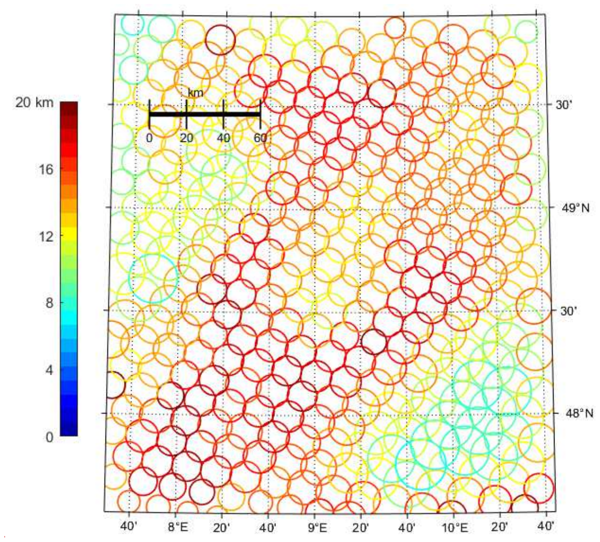

~~Figure 5: Spatial distribution of the mean soil moisture sampling distance in the model area required for keeping the maximum sampling error below 0.04 m³/m³ over the whole year. The circle diameter indicates the maximum sampling distance in the scale shown in the map, while its color (see color bar) gives the RMS of the maximum sampling distance over time for the year 2015.~~

~~brightness~~

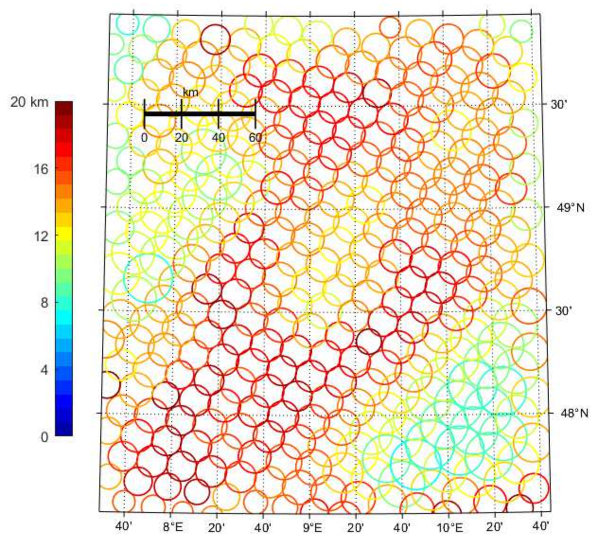

Figure 5: Spatial distribution of the mean of the maximum allowed soil moisture sampling distance in the model area required for keeping the maximum sampling error below 0.04 m^3/m^3 over the whole year. The circle radius indicates the maximum allowed sampling distance in the scale shown in the map, while its color (see color bar) gives the RMS of the maximum allowed sampling distance over time for the year 2015.

3.2 Brightness temperature

We now determine the maximum sampling distances for networks of ground-based microwave ~~radiometers observing the land surface required~~radiometer allowed to estimate SMOS/SMAP footprint brightness temperatures. To this goal, we transform the target accuracy of SMOS/SMAP soil moisture retrievals of 0.04 cm^3/cm^3 to the accuracy of the corresponding brightness temperature, which is approximately 10 K for H polarization and 5 K for V polarization according to CMEM forward simulations~~.~~ (Sabater et al., 2011;Monerris Belda, 2009). We note that this brightness temperature accuracy is not the instrument observing error of the (virtual) microwave radiometer, but the sensitivity of the microwave forward transfer model to soil moisture. We are aware, that the radiometric accuracies of ground-based and satellite-borne sensors are much better, and that the accuracy of the soil moisture-brightness temperature relation is mainly responsible for the retrieval accuracy; thus, we use the 10K/5K uncertainty only as a proxy for the overall error.

~~According to~~ By comparing the high-res TB for certain sampling distances with the antenna pattern TB from the satellite operator, Figure 6 ~~already~~shows different patterns to the soil moisture. Even at a

Formatted: Indent: First line: 1 cm

sampling distance of 800 m, the sampling error might exceed the 10K~~/~~ (5K) limit ~~at~~in certain regions and times. If we want to keep the limit with a probability of ~~90%~~only 75 percentiles (the upper boundary of the boxes in Figure 6~~ H/V~~, 100% confidence panels), ~~a~~the maximum sampling distance must stay below 4.4 km~~/4 km will confine the sampling error to below 10 K/5 K for H/V polarization brightness temperatures.~~. For ~~an average~~a sampling distance of 5.2 km, the error may go beyond the nominal 10 K~~/5 K for both polarizations already~~ (5 K) with a probability of 50~~%, and already for~~% For 9.2 km ~~average~~ sampling distance, and the maximum sampling error is always above the nominal values for some region and/or a day in the year. Even if we ~~relax~~require that the nominal error ~~to~~is undercut only with a probability of 70% ~~of~~for all pixels and days, ~~the requirement cannot be met already at 800 m average~~a sampling distance~~, while the average sampling distance required to fulfill the nominal accuracy for~~ of 800 m is not enough. If only 50% of all networks ~~moves from 5.2 to 10 km~~are required to fulfill the 10K/(5K) bound, a sampling distance of 10 km is sufficient.

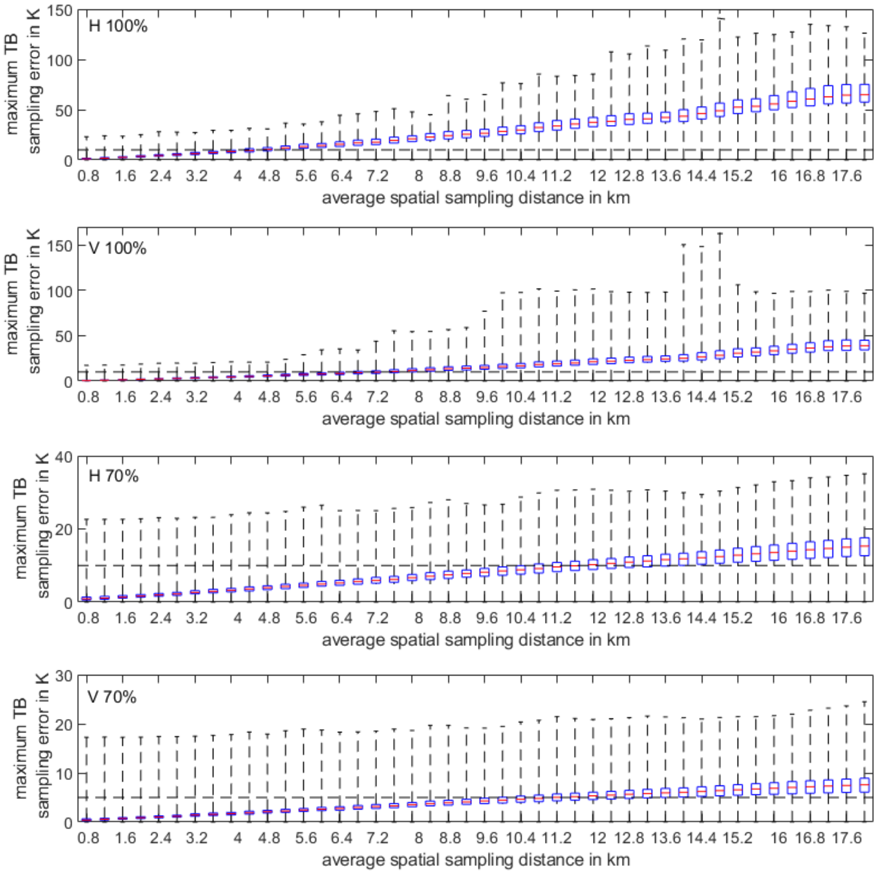

Figure 6: Same as Figure 3 but for the sampling error of the brightness temperature. The respective brightness temperature errors equivalent to a soil moisture accuracy of 0.04 cm^3/cm^3 of 10 K for H polarization and 5 K for V polarization are indicated as dashed horizontal lines.

The time series of the distribution of the maximum sampling distances for brightness temperature (Figure 7) is quite similar to the one for the maximum sampling distances for soil moisture. Figure 7 only illustrates the periods without freeze/thaw state transformations and liquid water in the soil dominate the brightness temperature signal. Values range from 6.8 km to 16.4 km for most cases. The spread of the sampling error has, however, a distinct seasonal variation; e.g., the maximum sampling distance for 90~~%~~ percent of the ~~sampling configurations~~footprints is 11.6 km from DOY 100 to 275 and 8.8 km for the rest of the year.

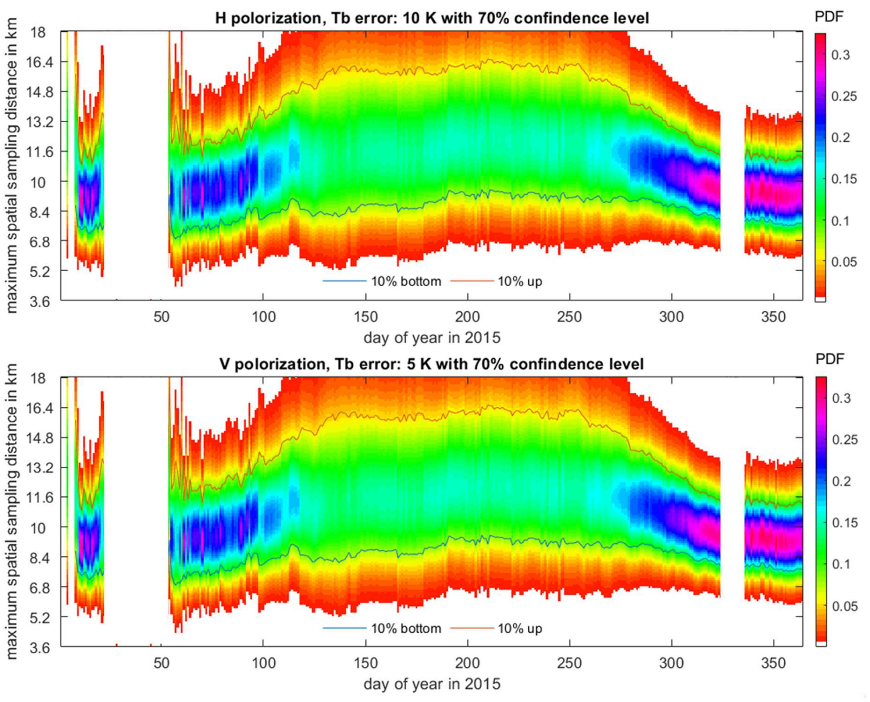

~~Figure 7: Time series of the distribution of maximum sampling distances (70% confidence in 10K/5K for H/V polorization) for brightness temperature at every sites in 2015. The degree of grayness indicates the probability of occurrence.~~

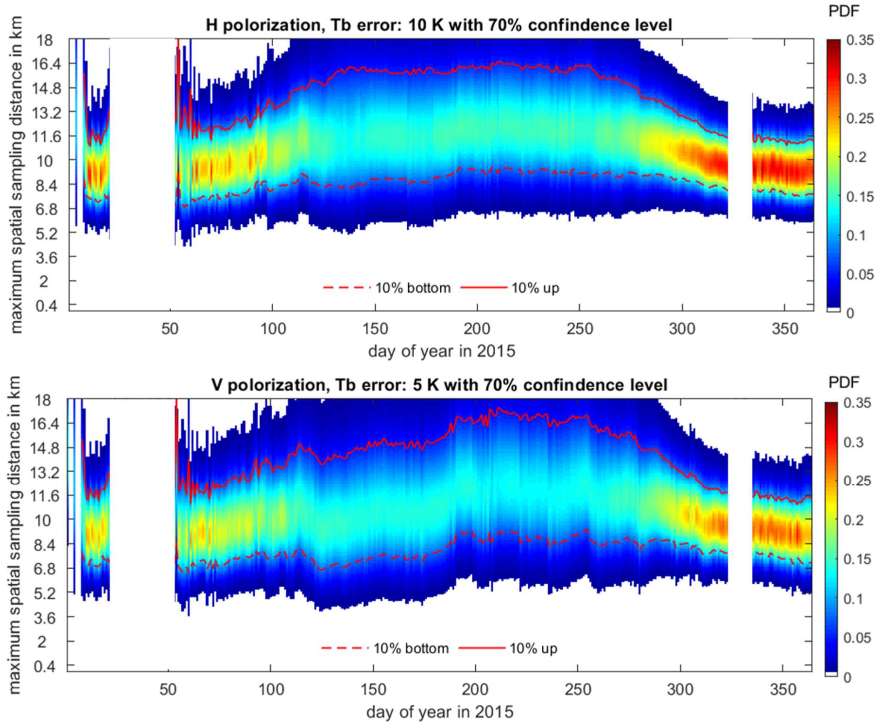

Figure 7: Time series of the distribution of maximum sampling distances (70% confidence in 10K/5K for H/V polorization) for brightness temperature at every sites in 2015. The color indicates the probability of occurrence.

The spatial distribution of the annual ~~average~~ maximum sampling distance ~~required~~allowed to guarantee a sampling error ~~below~~less than 10K/5K for H/V polarized brightness temperatures and its RMS for the year 2015 (Figure 8) are similar for H and V polarizations, but ~~show different and much stronger patterns~~shows a substantial spatial contrast compared to the results for soil moisture (Figure 5). ~~Similarly~~Again, the southeast corner of the model region ~~has~~allows for larger maximum sampling distances, but there are now also other distinct regions with larger ~~minimum~~allowed maximum sampling distances. Additional input parameters required - especially LAI - and internal parameters in CMEM ~~now~~additionally impact the representativeness of ~~different~~ sites ~~– especially LAI~~for brightness temperatures. LAI dominates the variation of the representativeness of ground-based observations and also its temporal variation, as can be inferred from the correlation between large maximum sampling distances with its variability over the year (correlation coefficient is 0.84/0.83 for H/V polarization), which is not observed for soil moisture. LAI is the only input in CMEM, which can lead to such a temporal variation because other~~ inputs and internal~~ parameters such as air temperature, soil moisture, soil properties, etc. are either fixed or do not impact ~~on~~as strongly the brightness temperature~~ significantly~~.

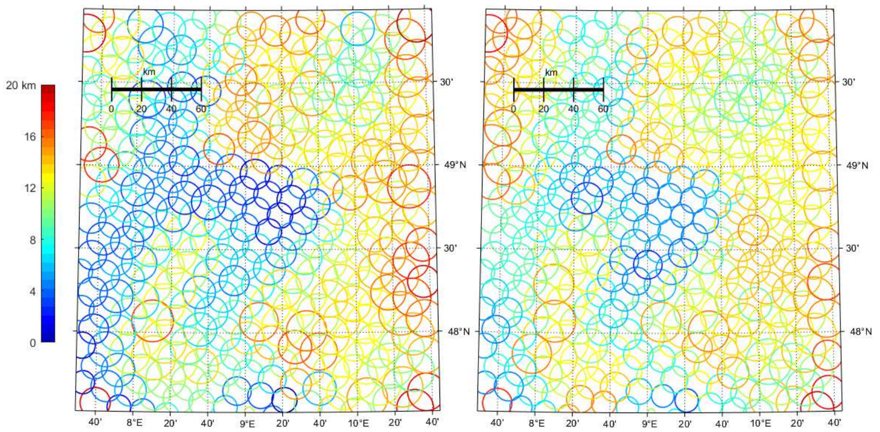

Figure 8: Spatial distribution of the maximum distances of stations (diameter of circles, see scale) for surface-based brightness temperature ~~network resolution~~observations required ~~in~~to keep the ~~model region. The circle diameter indicates the maximum~~ sampling ~~distance which keeps the~~ error below 10 K for H polarization (left panel) and 5 K for V polarization ~~in the scale shown in the map, while its~~(right

3.3 Maximum sampling distance differences between soil moisture and brightness temperature

The differences in the variability of the maximum allowed sampling distance for soil moisture and brightness temperature can be explained by using the microwave transfer model CMEM. The relationship between soil moisture and brightness temperature is complex and non-unique (Figure 9a, b). ~~E.g.,~~For example, a soil moisture value of ~~–~~0.4 cm^3/cm^3 ~~can relate~~relates to ~~a wide range of~~ brightness ~~temperature~~temperatures from 180 K to 250 K for H polarization and 225 K to 265 K for V polarization due to the variation of vegetation cover, soil properties, and terrain.

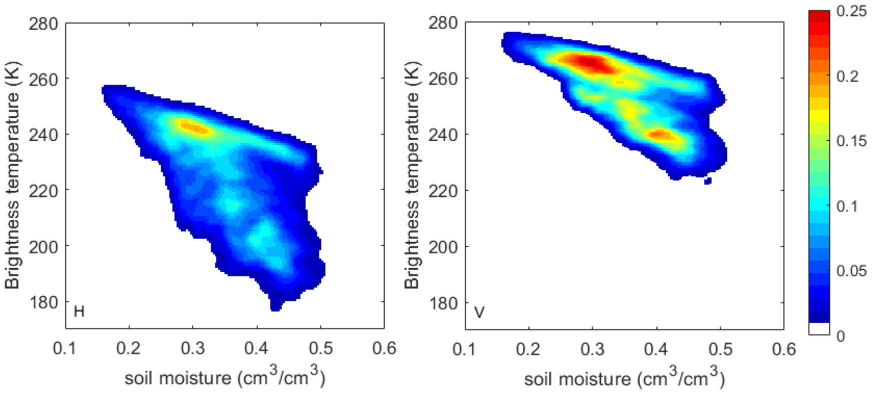

Figure 9: Scatter plots of the joint PDF between brightness temperature at H (left) and V (right) polarization against soil moisture computed from the 400 m resolution virtual reality for one year. Both the temporal and spatial variation ~~are accounted~~is included.

~~The~~As already mentioned in the introduction, the spatial resolution for the SMAP active product is 3 km and for the passive-active merged soil moisture product 9 km. SMAP CAL/VAL requires ~~for core stations 3~~three stations for the evaluation of the prior and ~~5~~five stations for the latter product~~.~~ (Colliander et al., 2017b). We computed the ~~average~~ station distance ~~for both products~~ required to keep the sampling error below the nominal 0.04 cm^3/cm^3 for both products by using the same methodology used above. Due to limited computation capacity, ~~not all~~only the higher-resolution ~~footprints are used, but only those~~pixels in the center of the 43-km SMOS footprints~~.~~ are evaluated. According to the results ~~displayed in~~ (Figure 10~~, the confidence level for most of~~), the ~~3/9~~ probability that 3 km ~~footprints~~and 9 km pixels sampled ~~by 3/5 stations~~with 3 and 5 stations, respectively, have sampling errors below the nominal value of 0.04 cm^3/cm^3 is below ~~50%-60~~40% and thus much lower than the required 70%. The temporal variation of the confidence level is larger for the 3 km than for the 9 km ~~footprints~~grid size.

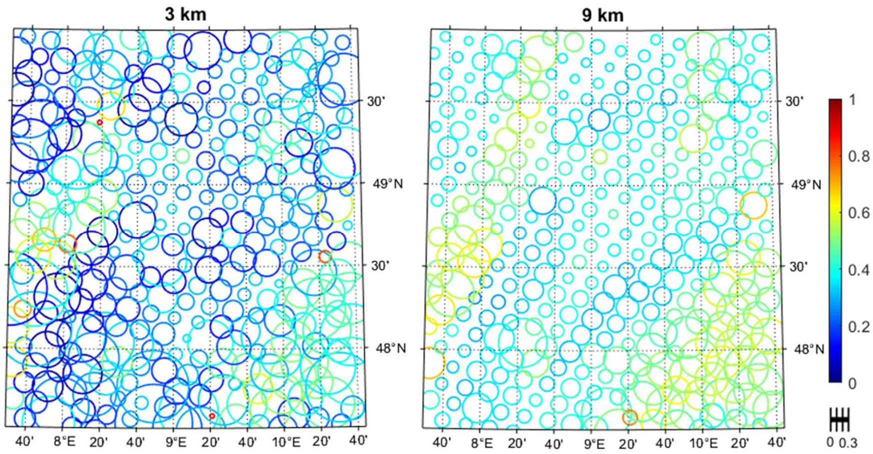

~~Figure 10: The spatial distribution of the soil moisture sampling confidence to achieve the 0.04 cm^3/cm^3 accuracy requirement by sampling 3/9 km footprints with 3/5 sites. The colors show the minimum confidence level throughout the year 2015 for every footprint. The size of circles indicate the standard deviation of the confidence level over the time.~~

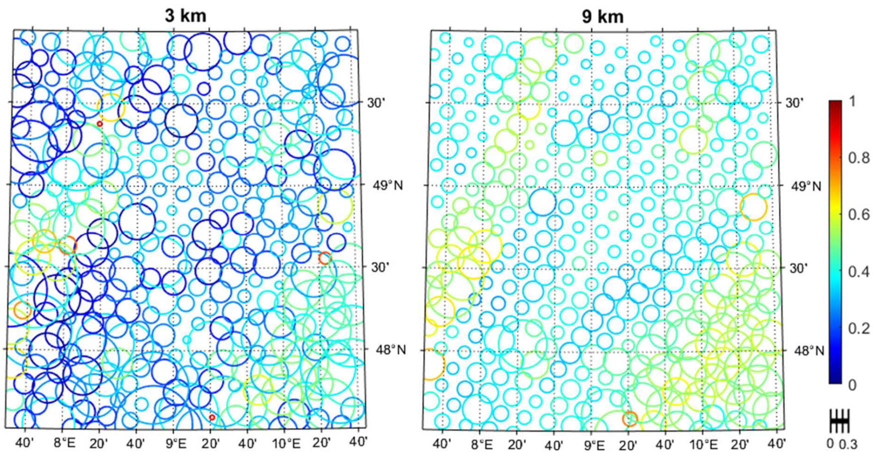

Figure 10: The spatial distribution of the soil moisture sampling confidence to achieve the 0.04 cm^3/cm^3 accuracy requirement by sampling 3 km (left) and 9 km footprints (right) with 3 and 5 sites, respectively (see the scale below the color bar). The colors show the minimum confidence level throughout the year 2015 for every footprint. The scale is soil moisture accuracy that can be achieved.

3.4 The impact of land surface inhomogeneity

Areas with vegetation water content ~~>~~above 5 kg/m^2 (mostly forests) are flagged in SMAP retrievals. The networks used in the studies by (Colliander et al., 2017b;~~ ~~Famiglietti et al., 2008) were selected ~~based on~~because of their relative homogeneity; thus, forested patches, open water, permanent ice and snow, urban areas, and wetlands are excluded. Soil moisture maps from SMAP/SMOS are, however, global. Thus estimates are provided everywhere; ~~thus~~hence, signals from open water surfaces on sub-grid scales may influence the products. We used our simulated observations to study the impact of sub-pixel contributions of forested areas on the sampling errors.

In total, only 16 of the 320 footprints ~~in~~covering the model area have forest fractions below 15% and negligible surface water contributions; such footprints are usually considered ~~as an~~ ideal ~~footprint~~ for soil moisture Cal/Val. ~~We compare their sampling statistics with the statistics for all footprints in Figure 11, which shows that in~~In terms of both soil moisture and brightness temperature, ~~the~~their maximum sampling errors ~~for the selected sites~~ are considerably lower compared to all sites for all sampling distances~~.~~ (Figure 11). Thus, excluding sites with larger forest fractions ~~above 15% is beneficial for both soil moisture and brightness temperature evaluations~~leads to lower sampling errors.

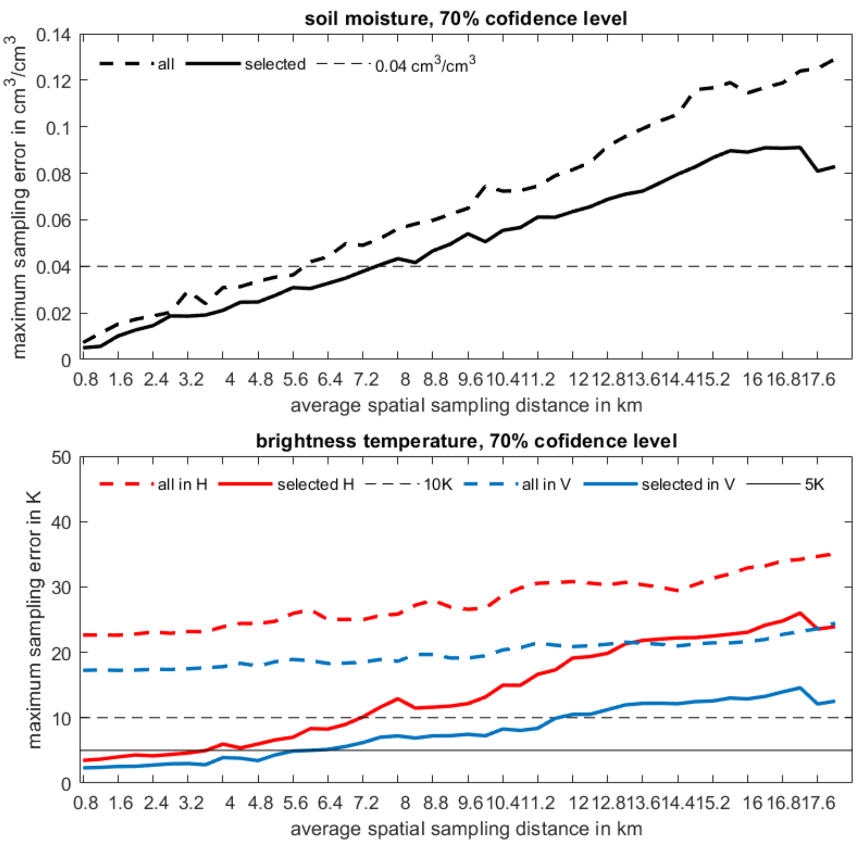

~~Figure 11: The maximum sampling errors of the arithmetic mean soil moisture/brightness temperature estimated from all sites and from sites with < 15% forest cover at given average sampling distances.~~

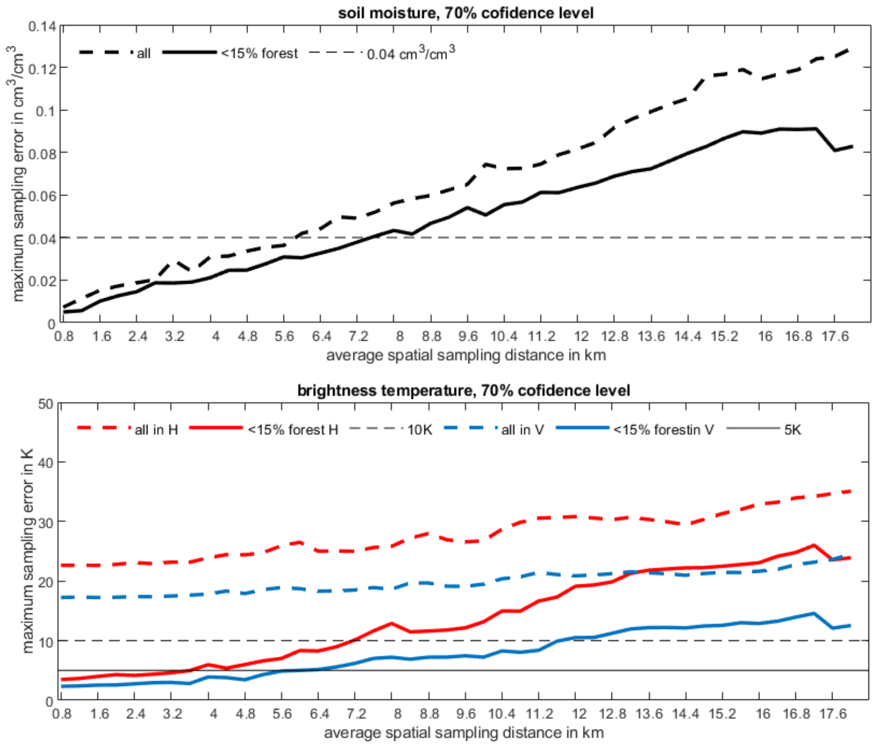

Figure 11: The maximum sampling errors of the arithmetic mean of soil moisture (top) and brightness temperature (bottom) estimated from all sites and from sites with forest cover below 15 % against average sampling distance.

The results shown in Figure 11 do not mean that forest sites always have higher soil moisture errors than non-forest sites, but by picking Cal/Val sites with favorable conditions reduces the required sampling density, which may, however, affect their representativeness. Moreover, the required sampling density inferred from non-forest sites cannot be extended to forest sites.

4. Conclusion and discussion

We used a virtual reality generated with ~~the~~a fully coupled subsurface-vegetation-atmosphere model platform ~~TerrSysMP~~ over southwestern Germany with a spatial resolution of 400 m for the land components to quantify the sampling error ~~of mean~~for the arithmetic averaged soil moisture and the weighted average brightness temperatures estimated from in-situ ground-based observation networks covering ~~the 43 km x 43 km~~ SMOS/SMAP-like footprints ~~over~~ of 43 km diameter for a wide range of potential ~~average~~ sampling distances. By using a ~~simulated~~ virtual reality at such ~~a~~ high resolution, we have a physically consistent three-dimensional evolution of the terrestrial system at our disposition~~,~~ from which we can take virtual soil moisture observations ~~at any resolution at and above 400 m,~~and – via the radiative transfer model CMEM and ~~we can simulate SMOS/SMAP-like observations taking into account the~~ a satellite antenna function ~~and the~~ – microwave ~~radiative transfer model CMEM.~~

~~A comparison between the representativeness of ground-based soil moisture and~~ brightness temperature ~~observation networks reveals the complexity behind the sampling density issue.~~ observations from the highest resolution at 400 m to any larger resolution.

We adopted as an upper threshold for the sampling error of ~~the estimated soil moisture and brightness temperature for~~ground-based sensor networks when estimating averages over SMOS/SMAP pixels the target SMOS/SMAP soil moisture retrieval accuracy of 0.04 cm^3/cm^3. We quantified the maximum sampling distance ~~of ground-based observations required to keep~~, which still keeps the sampling error below that accuracy either for all ~~and~~or for 70% of ~~the~~all SMOS/SMAP pixels ~~over~~in the modeling region ~~and~~ over one year for all network configurations possible ~~for the specified average sampling distances~~. A major assumption in our study is, that the estimation of soil moisture for an area with a diameter of about 400 m is possible, or in other words that a single station within a 400-m area is representative for its spatial average, an assumption also discussed in Famiglietti et al. (2008). Compared to the region analyzed in Famiglietti et al. (2008), our study uses a much more realistic terrain and excludes subjective factors in selecting suitable Cal/Val sites. Because of this, the soil moisture error in our study grows much faster with increasing sampling distance. We also find that the estimation of area-averaged brightness temperatures from a network of ground-based stations has a different error growth with increasing sampling distance compared to soil moisture despite an initial linear growth for both of them (compare Figures 3 and 6). Thus, a representative soil moisture network does not guarantee a representative radiometer network for the estimation of area-averaged brightness temperature, or that brightness temperatures computed for the soil moisture stations can be used for that estimate. But Figure 3 and 6 also show, that sampling distances below 6 km still fulfill the 70^{th} percentage requirement for keeping the sampling error below the nominal error.

Besides plant types, there is no clear pattern similarity between clay/sand/elevation (Figure 1) and spatial sampling distance (Figure 5). Soil properties may be related to the regional climate (annual precipitation, radiation flux balance, etc.). For instance, arid regions usually contain higher sand fractions, but such regions are seldom the focus of soil moisture studies because of its low variation. Transition zones like our model area usually encompass various soil properties, which are often correlated with landuse and vegetation and thus the plant function type used in the CLM. Topography also affects the soil moisture and TB distribution, but it is difficult to infer the impact of landuse and vegetation because soil properties determine both the water holding capacity and the plant cover. In practice, soil moisture monitoring networks avoid complex terrain. Homogenous terrain and landscape lead to an overestimation of satellite soil moisture product accuracies.

The statistical results in our study differ from those in Famiglietti et al. (2008) because our focus is on the satellite footprint scale and not the representativeness of one station within a network. For example, a particular sensor may not represent the true 400 m average, but one such sensor every 400 m may statistically sufficiently represent a much larger footprint. A similar concept is adapted in ensemble forecasts using members, e.g., with different physics packages, none of which is expected to be the truth (Lewis, 2005; Leutbecher and Palmer, 2008). The space detected by a soil moisture sensor, which is measuring the dielectric constant of the soil or other media using capacitance/frequency domain technology, is about a ten-centimeter sphere. Thus, the study by Famiglietti et al. (2008) assumes soil moisture homogeneity on the scale of meters. We believe that the 400-m soil moisture homogenous assumption does not interfere with our conclusions and that our study can be considered as a complement to the study by Famiglietti et al. (2008).

The calibration and validation of ~~L-band~~ passive ~~remote sensing of~~satellite-based L-band soil moisture ~~is~~estimates are difficult due to ~~its~~the large sub-pixel variability (Lv et al., 2019; Lv et al., 2016b). Even with a perfect microwave transfer model and perfect sensors, we can hardly find ~~a~~an appropriate in-situ observation to compare with. While soil moisture also varies in the vertical, sensors are usually mounted at a fixed depth; thus, comparisons with satellite observations require the knowledge of the microwave penetration depth, which is, however, unknown in general. (Lv et al~~. (~~., 2018) developed a model based on the soil effective temperature, which sheds light on this fundamental problem. This study isolates the sampling density issue from other factors and is a test of the current Cal/Val network standard without pre-knowledge of the site. The SMAP team suggests 15 sites for a 36 km by 36 km ~~footprint,~~grid-size (Colliander et al., 2017b), and this study agrees with this configuration for typical ~~midlatitude~~mid-latitude European regions~~.~~ from the sampling error perspective. For a 36 km by 36 km grid-size, the required sampling sites would ranges from about 36 (6 km) to 4 (17 km). However, ~~5~~five sites for 9 km by 9 km and ~~3~~three sites for 3 km by 3 km will miss the 70 % confidence level requirements over this area. Since SMAP's 9-km and 3-km soil moisture products are from a combination of passive and active microwave signals, which has lower accuracy than the passive one(Entekhabi et al., 2010), their Cal/Val campaigns shall determine sampling distances with less confidence level.

~~It is difficult~~Our virtual reality contains extensive land cover variability (Figure 1), thus it would be helpful to ~~set up an observation network, which represents~~ adopt our approach for less complex regions with variabilities closer to the ~~whole satellite footprint precisely. We~~ typical Cal/Val station networks. Overall, we find that a~~ maximum~~ soil moisture sampling distance ~~of~~ roughly below 3 km ~~if we want~~is necessary to ~~be 100% sure that~~keep the sampling ~~error is~~errors always below the nominal value~~ of 0.04~~ ~~cm^3/cm^3. If we allow~~. The allowance for a failure probability of 30 % ~~a maximum sampling~~extends this distance ~~of~~to 10 km~~ is sufficient.~~. For brightness temperatures, the sampling ~~requirement is~~requirements are much ~~stricter, because~~more strict; already at 800 m sampling distance, it cannot be guaranteed~~,~~ that the sampling error remains below the equivalent threshold of 10K/5K for H and V-polarization, respectively, even when allowing for a 30% probability of failure. The error sources in retrieving soil moisture from TB data is also large in reality but not concerned in this study because VR01 and the TB produced by CMEM exclude the uncertainty except the sampling distance.

Our results are not only useful for the planning of ground-based soil moisture networks, they also contribute to a better understanding of the relation between brightness temperatures observed at the ground – or simulated at high resolution - and the ones observed from satellites apart from non-linearity effects of radiative transfer (e.g.,(Drusch et al., 1999)). The study allows, e.g., to quantify to what extent a bias between satellites brightness temperature and forward simulation could be explained by the spatial sampling (e.g., Figures 5, 8, and 11), and to understand the similarities and dissimilarities between observed soil moisture and brightness temperature time-series (Figures 4 and 7). Since ground-based soil moisture networks will always cover only certain parts of a satellite pixel, a bias must be expected between both. Biases in satellite and ground-based estimates of soil moisture can also be caused by the different representativeness of the latter for soil moisture and brightness temperatures.

While the ~~required~~allowed maximum sampling distances do not change much over the year for soil moisture - except after large-scale precipitation events which allow for larger sampling distances - its equivalent for brightness temperature has a strong seasonal variation because of the blurring effect of vegetation during the growing season when brightness temperatures become more homogeneous. The spatial distribution of the maximum sampling distances and their local variances behave quite differently between soil moisture and brightness temperature. The spatial patterns are different, and while the maximum allowed sampling distance and its variance are strongly related for brightness temperature, they are barely related for soil moisture; this different behavior is caused by the complexity of other factors influencing microwave radiative transfer.

Our study strongly suggests that the sampling density of current SMOS/SMAP ground-based Cal/Val networks ~~should be reviewed carefully~~ and the resulting potential sampling error of estimated pixel-mean soil moisture and brightness temperatures considered in such studies~~.~~ should be reviewed carefully. We expect this study will help to ~~better~~ understand the errors of satellite-derived soil moisture better.

Acknowledgments

This research was funded by the Deutsche Forschungsgemeinschaft (DFG) via FOR2131: "Data Assimilation for Improved Characterization of Fluxes across Compartmental Interfaces", subproject P2. Compute time has been provided by the Gauss Centre for Supercomputing (http://www.gauss-centre.eu/gauss-centre/EN/Home/home_node.html) operated by the Juelich Supercomputing Centre (http://www.fz-juelich.de/ias/jsc/EN/Home/home_node.html). We thank the members of HPSC-TerrSys (http://www.hpsc-terrsys.de/hpsc-terrsys/EN/Home/home_node.html) and Klaus Goergen in particular for invaluable technical support with the JUQUEEN supercomputer. Furthermore, we thank Prabhakar Shresta and Mauro Sulis from the Transregional Collaborative Research Center 32 (TR32) for their preliminary work and introduction to the TerrSysMP modeling platform.

References

Ashby, S. F., and Falgout, R. D.: A parallel multigrid preconditioned conjugate gradient algorithm for groundwater flow simulations, Nucl Sci Eng, 124, 145-159, 1996.

Baldauf, M., Seifert, A., Förstner, J., Majewski, D., Raschendorfer, M., and Reinhardt, T.: Operational convective-scale numerical weather prediction with the COSMO model: Description and sensitivities, Monthly Weather Review, 139, 3887-3905, 2011.

Baroni, G., Zink, M., Kumar, R., Samaniego, L., and Attinger, S.: Effects of uncertainty in soil properties on simulated hydrological states and fluxes at different spatio-temporal scales, Hydrol. Earth Syst. Sci., 21, 2301-2320, 10.5194/hess-21-2301-2017, 2017.

Bhuiyan, H. A. K. M., McNairn, H., Powers, J., Friesen, M., Pacheco, A., Jackson, T. J., Cosh, M. H., Colliander, A., Berg, A., Rowlandson, T., Bullock, P., and Magagi, R.: Assessing SMAP Soil Moisture Scaling and Retrieval in the Carman (Canada) Study Site, Vadose Zone J, 17, ARTN 180132

10.2136/vzj2018.07.0132, 2018.

Brocca, L., Melone, F., Moramarco, T., and Morbidelli, R.: Spatial-temporal variability of soil moisture and its estimation across scales, Water Resources Research, 46, ~~10.1029/2009wr008016, 2010.~~Artn W02516

~~Brown~~10.1029/2009wr008016, 2010.

Burgin, M. ~~A~~S., Colliander, A., ~~Torres~~Njoku, E. G., Chan, S. K., Cabot, F., ~~Corbella, I~~Kerr, Y. H., Bindlish, R., Jackson, T. J., Entekhabi, D., and ~~Colliander, A.: SMOS calibration~~Yueh, S. H.: A Comparative Study of the SMAP Passive Soil Moisture Product With Existing Satellite-Based Soil Moisture Products, Ieee Transactions on Geoscience and Remote Sensing, ~~46, 646-658, Doi~~55, 2959-2971, 10.1109/Tgrs.~~2007.914810, 2008~~2017.2656859, 2017.

Chen, F., Crow, W. T., Colliander, A., Cosh, M. H., Jackson, T. J., Bindlish, R., Reichle, R. H., Chan, S. K., Bosch, D. D., Starks, P. J., Goodrich, D. C., and Seyfried, M. S.: Application of Triple Collocation in Ground-Based Validation of Soil Moisture Active/Passive (SMAP) Level 2 Data Products, Ieee Journal of Selected Topics in Applied Earth Observations and Remote Sensing, 10, 489-502, 10.1109/Jstars.2016.2569998, 2017.

Chen, F., Crow, W. T., Bindlish, R., Colliander, A., Burgin, M. S., Asanuma, J., and Aida, K.: Global-scale evaluation of SMAP, SMOS and ASCAT soil moisture products using triple collocation, Remote Sensing of Environment, 214, 1-13, 10.1016/j.rse.2018.05.008, 2018.

Colliander, A., Cosh, M. H., Misra, S., Jackson, T. J., Crow, W. T., Chan, S., Bindlish, R., Chae, C., Collins, C. H., and Yueh, S. H.: Validation and scaling of ~~soil moisture~~soilmoisture in a semi-arid environment: SMAP validation experiment 2015 (SMAPVEX15), Remote Sensing of Environment, 196, 101-112, 10.1016/j.rse.2017.04.022, 2017a.

Colliander, A., Jackson, T. J., Bindlish, R., Chan, S., Das, N., Kim, S. B., Cosh, M. H., Dunbar, R. S., Dang, L., Pashaian, L., Asanuma, J., Aida, K., Berg, A., Rowlandson, T., Bosch, D., Caldwell, T., Caylor, K., Goodrich, D., al Jassar, H., Lopez-Baeza, E., Martínez-Fernández, J., González-Zamora, A., Livingston, S., McNairn, H., Pacheco, A., Moghaddam, M., Montzka, C., Notarnicola, C., Niedrist, G., Pellarin, T., Prueger, J., Pulliainen, J., Rautiainen, K., Ramos, J., Seyfried, M., Starks, P., Su, Z., Zeng, Y., van der Velde, R., Thibeault, M., Dorigo, W., Vreugdenhil, M., Walker, J. P., Wu, X., Monerris, A., O'Neill, P. E., Entekhabi, D., Njoku, E. G., and Yueh, S.: Validation of SMAP surface soil moisture products with core validation sites, Remote Sensing of Environment, 191, 215-231, https://doi.org/10.1016/j.rse.2017.01.021, 2017b.

Formatted: Font: Bold

Formatted: Space After: 8 pt

Coopersmith, E. J., Cosh, M. H., Bell, J. E., Kelly, V., Hall, M., Palecki, M. A., and Temimi, M.: Deploying temporary networks for upscaling of sparse network stations, Int. J. Appl. Earth Obs. Geoinf., 52, 433-444, 10.1016/j.jag.2016.07.013, 2016.

Cosh, M. H., Jackson, T. J., Starks, P., Bosch, D., Collins, C. H., Seyfried, M., Prueger, J., Livingston, S., and Bindlish, R~~., and Prueger, J. H.: Watershed scale temporal and spatial stability of soil moisture and its role in~~ .: Strategies for validating satellite ~~estimates,~~ soil moisture products using in situ networks: Lessons from the USDA-ARS watersheds, 2017 IEEE International Geoscience and Remote Sensing ~~of Environment, 92, 427-435, 10.1016/j.rse.2004.02.016, 2004.~~Symposium (IGARSS), 2017, 2015-2018,

Crow, W. T., Berg, A. A., Cosh, M. H., Loew, A., Mohanty, B. P., Panciera, R., de Rosnay, P., Ryu, D., and Walker, J. ~~P.: Upscaling sparse ground-based soil moisture observations for the validation of coarse-resolution satellite soil moisture products~~P.: UPSCALING SPARSE GROUND-BASED SOIL MOISTURE OBSERVATIONS FOR THE VALIDATION OF COARSE-RESOLUTION SATELLITE SOIL MOISTURE PRODUCTS, Reviews of Geophysics, 50, 20, 10.1029/2011rg000372, 2012.

dall'Amico, J. T., Schlenz, F., Loew, A., and Mauser, W.: First Results of SMOS Soil Moisture Validation in the Upper Danube Catchment, Ieee Transactions on Geoscience and Remote Sensing, 50, 1507-1516, 10.1109/Tgrs.2011.2171496, 2012.

de Rosnay, P., Calvet, J. C., Kerr, Y., Wigneron, J. P., Lemaitre, F., Escorihuela, M. J., Sabater, J. M., Saleh, K., Barrie, J. L., Bouhours, G., Coret, L., Cherel, G., Dedieu, G., Durbe, R., Fntz, N. E. D., Froissard, F., Hoedjes, J., Kruszewski, A., Lavenu, F., Suquia, D., and Waldteufel, P.: SMOSREX: A long term field campaign experiment for soil moisture and land surface processes remote sensing, Remote Sensing of Environment, 102, 377-389, 10.1016/j.rse.2006.02.021, 2006.

Delwart, S., Bouzinac, C., Wursteisen, P., Berger, M., Drinkwater, M., Martin-Neira, M., and Kerr, Y. H.: SMOS validation and the COSMOS campaigns, Ieee Transactions on Geoscience and Remote Sensing, 46, 695-704, 2008.

Dorigo, W. A., Wagner, W., Hohensinn, R., Hahn, S., Paulik, C., Xaver, A., Gruber, A., Drusch, M., Mecklenburg, S., van Oevelen, P., Robock, A., and Jackson, T.: The International Soil Moisture Network: a data hosting facility for global in situ soil moisture measurements, Hydrology and Earth System Sciences, 15, 1675-1698, 10.5194/hess-15-1675-2011, 2011.

Drusch, M., Wood, E. F., and Simmer, C.: Up-scaling effects in passive microwave remote sensing: ESTAR 1.4 GHz measurements during SGP '97, Geophysical Research Letters, 26, 879-882, Doi 10.1029/1999gl900150, 1999.

Entekhabi, D., Njoku, E. G., O'Neill, P. E., Kellogg, K. H., Crow, W. T., Edelstein, W. N., Entin, J. K., Goodman, S. D., Jackson, T. J., Johnson, J., Kimball, J., Piepmeier, J. R., Koster, R. D., Martin, N., McDonald, K. C., Moghaddam, M., Moran, S., Reichle, R., Shi, J. C., Spencer, M. W., Thurman, S. W., Tsang, L., and Van Zyl, J.: The Soil Moisture Active Passive (SMAP) Mission, P Ieee, 98, 704-716, 10.1109/jproc.2010.2043918, 2010.

Famiglietti, J. S., Ryu, D. R., Berg, A. A., Rodell, M., and Jackson, T. J.: Field observations of soil moisture variability across scales, Water Resources Research, 44, ~~10.1029/2006wr005804, 2008.~~Artn W01423 10.1029/2006wr005804, 2008.

Gasper, F., Goergen, K., Shrestha, P., Sulis, M., Rihani, J., Geimer, M., and Kollet, S.: Implementation and scaling of the fully coupled Terrestrial Systems Modeling Platform (TerrSysMP v1. 0) in a massively parallel supercomputing environment–a case study on JUQUEEN (IBM Blue Gene/Q), Geosci. Model Dev., 7, 2531-2543, 2014.

Jackson, T., Colliander, A., Kimball, J., Reichle, R., Crow, W., Entekhabi, D., and Neill, P.: Science data calibration and validation plan, Jet Propuls. Lab, 2012.

Kerr, Y. H., Waldteufel, P., Wigneron, J. P., Delwart, S., Cabot, F., Boutin, J., Escorihuela, M. J., Font, J., Reul, N., Gruhier, C., Juglea, S. E., Drinkwater, M. R., Hahne, A., Martin-Neira, M., and Mecklenburg, S.:

The SMOS Mission: New Tool for Monitoring Key Elements of the Global Water Cycle, P Ieee, 98, 666-687, Doi 10.1109/Jproc.2010.2043032, 2010.

Kerr, Y. H., Al-Yaari, A., Rodriguez-Fernandez, N., Parrens, M., Molero, B., Leroux, D., Bircher, S., Mahmoodi, A., Mialon, A., Richaume, P., Delwart, S., Al Bitar, A., Pellarin, T., Bindlish, R., Jackson, T. J., Rudiger, C., Waldteufel, P., Mecklenburg, S., and Wigneron, J. P.: Overview of SMOS performance in terms of global soil moisture monitoring after six years in operation, Remote Sensing of Environment, 180, 40-63, 10.1016/j.rse.2016.02.042, 2016.

Kollet, S. J., Maxwell, R. M., Woodward, C. S., Smith, S., Vanderborght, J., Vereecken, H., and Simmer, C.: Proof of concept of regional scale hydrologic simulations at hydrologic resolution utilizing massively parallel computer resources, Water Resources Research, 46, 2010.

Lawrence, P. J., and Chase, T. N.: Representing a new MODIS consistent land surface in the Community Land Model (CLM 3.0), Journal of Geophysical Research: Biogeosciences, 112, 2007.

~~Lemaitre, F., Poussiere, J. C., Kerr, Y. H., Dejus, M., Durbe, R., de Rosnay, P., and Calvet, J. C.: Design and test of the ground-based L-band radiometer for estimating water in soils (LEWIS), Ieee Transactions on Geoscience and Remote Sensing, 42, 1666-1676, 10.1109/tgrs.2004.831230, 2004.~~

Lv, S., Wen, J., Zeng, Y., Tian, H., and Su, Z.: An improved two-layer algorithm for estimating effective soil temperature in microwave radiometry using in situ temperature and soil moisture measurements, Remote Sensing of Environment, 152, 356-363, http://dx.doi.org/10.1016/j.rse.2014.07.007, 2014.

Lv, S., Zeng, Y., Wen, J., and Su, Z.: A reappraisal of global soil effective temperature schemes, Remote Sensing of Environment, 183, 144-153, ~~10.1016/j.rse.2016.05.012,~~http://dx.doi.org/10.1016/j.rse.2016.05.012, 2016a.

Lv, S., Zeng, Y., Wen, J., Zheng, D., and Su, Z.: Determination of the Optimal Mounting Depth for Calculating Effective Soil Temperature at L-Band: Maqu Case, Remote Sensing, 8, 476, 2016b.

Lv, S., Zeng, Y., Wen, J., Zhao, H., and Su, Z.: Estimation of Penetration Depth from Soil Effective Temperature in Microwave Radiometry, Remote Sensing, 10, 519, 2018.

Lv, S., Zeng, Y., Su, Z., and Wen, J.: A Closed-Form Expression of Soil Temperature Sensing Depth at L-Band, IEEE Transactions on Geoscience and Remote Sensing, 1-9, 10.1109/TGRS.2019.2893687, 2019.

Molero, B., Leroux, D. J., Richaume, P., Kerr, Y. H., Merlin, O., Cosh, M. H., and Bindlish, R.: Multi-Timescale Analysis of the Spatial Representativeness of In Situ Soil Moisture Data within Satellite Footprints, Journal of Geophysical Research-Atmospheres, 123, 3-21, 10.1002/2017jd027478, 2018.

Monerris Belda, A.: Experimental estimation of soil emissivity and its application to soil moisture retrieval in the SMOS mission, 2009.

Montzka, C., Bogena, H. R., Weihermuller, L., Jonard, F., Bouzinac, C., Kainulainen, J., Balling, J. E., Loew, A., Dall'Amico, J. T., Rouhe, E., Vanderborght, J., and Vereecken, H.: Brightness Temperature and Soil Moisture Validation at Different Scales During the SMOS Validation Campaign in the Rur and Erft Catchments, Germany, Ieee Transactions on Geoscience and Remote Sensing, 51, 1728-1743, 10.1109/Tgrs.2012.2206031, 2013.

Njoku, E. G., and Kong, J.-A.: Theory for passive microwave remote-sensing of near-surface soil-moisture, Journal of Geophysical Research, 82, 3108-3118, 1977.

O'Neill, P., Chan, S., Njoku, E., Jackson, T., and Bindlish, R.: Soil Moisture Active Passive (SMAP), Algorithm Theoretical Basis Document ~~Level 2 & 3 Soil Moisture (Passive) Data Products, Revision B, 2015.~~

Level 2 & 3 Soil Moisture (Passive) Data Products, Revison B, 2015.

Ochsner, T. E., Cosh, M. H., Cuenca, R. H., Dorigo, W. A., Draper, C. S., Hagimoto, Y., Kerr, Y. H., Larson, K. M., Njoku, E. G., Small, E. E., and Zreda, M.: State of the Art in Large-Scale Soil Moisture Monitoring, Soil Sci Soc Am J, 77, 1888-1919, 10.2136/sssaj2013.03.0093, 2013.

Formatted: Space After: 8 pt

Oleson, K., Niu, G. Y., Yang, Z. L., Lawrence, D., Thornton, P., Lawrence, P., Stöckli, R., Dickinson, R., Bonan, G., and Levis, S.: Improvements to the Community Land Model and their impact on the hydrological cycle, Journal of Geophysical Research: Biogeosciences, 113, 2008.

Qin, J., Yang, K., Lu, N., Chen, Y. Y., Zhao, L., and Han, M. L.: Spatial upscaling of in-situ soil moisture measurements based on MODIS-derived apparent thermal inertia, Remote Sensing of Environment, 138, 1-9, 10.1016/j.rse.2013.07.003, 2013.

Rosnay, P. d., Drusch, M., and Sabater, J. ı. M. n.: Milestone 1 Tech Note - Part 1: SMOS Global Surface Emission Model, 2009.

Sabater, J. M., De Rosnay, P., and Balsamo, G.: Sensitivity of L-band NWP forward modelling to soil roughness, International Journal of Remote Sensing, 32, 5607-5620, 10.1080/01431161.2010.507260, 2011.

Schalge, B., Rihani, J., Baroni, G., Erdal, D., Geppert, G., Haefliger, V., Haese, B., Saavedra, P., Neuweiler, I., Hendricks Franssen, H. J., Ament, F., Attinger, S., Cirpka, O. A., Kollet, S., Kunstmann, H., Vereecken, H., and Simmer, C.: High-Resolution Virtual Catchment Simulations of the Subsurface-Land Surface-Atmosphere System, Hydrol. Earth Syst. Sci. Discuss., 2016, 1-44, 10.5194/hess-2016-557, 2016.

Schalge, B., Haefliger, V., Kollet, S., and Simmer, C.: Improvement of surface run-off in the hydrological model ParFlow by a scale-consistent river parameterization, Hydrol Process, 33, 2006-2019, 10.1002/hyp.13448, 2019.

Shrestha, P., Sulis, M., Masbou, M., Kollet, S., and Simmer, C.: A Scale-Consistent Terrestrial Systems Modeling Platform Based on COSMO, CLM, and ParFlow, Monthly Weather Review, 142, 3466-3483, 10.1175/mwr-d-14-00029.1, 2014.

Sulis, M., Langensiepen, M., Shrestha, P., Schickling, A., Simmer, C., and Kollet, S. J.: Evaluating the influence of plant-specific physiological parameterizations on the partitioning of land surface energy fluxes, Journal of ~~Hydrometeorology~~hydrometeorology, 16, 517-533, 2015.

Tian, Y., Dickinson, R., Zhou, L., Zeng, X., Dai, Y., Myneni, R., Knyazikhin, Y., Zhang, X., Friedl, M., and Yu, H.: Comparison of seasonal and spatial variations of leaf area index and fraction of absorbed photosynthetically active radiation from Moderate Resolution Imaging Spectroradiometer (MODIS) and Common Land Model, Journal of Geophysical Research: Atmospheres, 109, 2004.

Ulaby, F. T., Moore, R. K., and Fung, A. K.: Microwave Remote Sensing Active and Passive-Volume III: From Theory to Applications, Artech House, Inc, 1986.

Vereecken, H., Huisman, J. A., Bogena, H., Vanderborght, J., Vrugt, J. A., and Hopmans, J. W.: On the value of soil moisture measurements in vadose zone hydrology: A review, Water Resources Research, 44, ~~10.1029/2008wr006829, 2008.~~W00d06

10.1029/2008wr006829, 2008.

Zeng, X., Shaikh, M., Dai, Y., Dickinson, R. E., and Myneni, R.: Coupling of the common land model to the NCAR community climate model, Journal of Climate, 15, 1832-1854, 2002.

Formatted: Space After: 8 pt

Formatted: Space After: 0 pt